CSIRO PUBLISHING

www.publish.csiro.au/journals/ijwf *International Journal of Wildland Fire*, 2007, **16**, 1–22

A physics-based approach to modelling grassland fires

William Mell[A,E], *Mary Ann Jenkins*[B], *Jim Gould*[C,D] *and Phil Cheney*[C]

[A]Building and Fire Research Laboratory, National Institute of Standards and Technology, Gaithersburg, MD 20899-8663, USA.

[B]Department of Earth and Space Science and Engineering, York University, Toronto, ON M3J 1P3, Canada.

[C]Ensis-Forest Biosecurity and Protection, CSIRO, Kingston, ACT 2604, Australia.

[D]Bushfire Cooperative Research Centre, East Melbourne, Vic. 3002, Australia.

[E]Corresponding author. Email: ruddy@nist.gov

Abstract. Physics-based coupled fire–atmosphere models are based on approximations to the governing equations of fluid dynamics, combustion, and the thermal degradation of solid fuel. They require significantly more computational resources than the most commonly used fire spread models, which are semi-empirical or empirical. However, there are a number of fire behaviour problems, of increasing relevance, that are outside the scope of empirical and semi-empirical models. Examples are wildland–urban interface fires, assessing how well fuel treatments work to reduce the intensity of wildland fires, and investigating the mechanisms and conditions underlying blow-up fires and fire spread through heterogeneous fuels. These problems are not amenable to repeatable full-scale field studies. Suitably validated coupled atmosphere–fire models are one way to address these problems. This paper describes the development of a three-dimensional, fully transient, physics-based computer simulation approach for modelling fire spread through surface fuels. Grassland fires were simulated and compared to findings from Australian experiments. Predictions of the head fire spread rate for a range of ambient wind speeds and ignition line-fire lengths compared favourably to experiments. In addition, two specific experimental cases were simulated in order to evaluate how well the model predicts the development of the entire fire perimeter.

Additional keywords: computational fluid dynamics, fire spread, numerical simulation, wildland fire.

Introduction and background

Wildfires and wildland–urban interface (WUI) fires are driven by complex physical and chemical processes, operating on vastly different scales, whose interactions depend on coupling between the atmosphere, topography, fire, and solid fuels. Both wildland and WUI fires are very difficult, if not impossible, to study with full-scale repeatable experiments in the field due to their expense, safety implications, and variations in atmosphere, terrain, and fuel conditions. Yet, there has been a long-standing need to improve our understanding of these fires (Williams 1982). Forests are strongly connected to the wildfire regime, and their nature is dependent on the frequency, extent, and severity of forest fires. Reconciling the need to protect forest lands that are valuable for industry and recreation with the natural role of fire in maintaining forest ecosystems is a priority in developing fire management in Canada. Both fire occurrence and average annual area burned by Canadian forest fires have increased over the past three decades. The records indicate 6000 fires per year in the period 1930–1960 to almost 10 000 fires per year during the 1980s and 1990 (Murphy *et al.* 2000), where the change in fire occurrence is attributed to a growing population, expanded forest use, and an increased detection capability (Stock and Simard 1993).

Studies in the United States (USDA Forest Service 2006) suggest that as a consequence of the past wildfire management practice of total suppression, many of America's forests have accumulations of historic dense, dead fallen vegetation. It is maintained that this, along with (and possibly dominated by) climate change in the Western United States (Westerling *et al.* 2006), has made forests more dangerous from a fire safety perspective and weakened ecologically; fires ignite more quickly, burn with greater intensity, and spread more rapidly than in the past. According to the US General Accountability Office, in the 1990s the number and size of wildfires, and the associated fire fighting cost, has increased dramatically (GAO 1999). In the United States forest fires are an increasing threat to lives and property. The number of homes at risk of fire in the WUI is also likely to increase due to the growing number of people moving into fire-prone areas (GAO 2005). Based on 2000 census information 36% of homes in the United States are within the WUI (Stewart *et al.* 2003). In California alone, homes in the WUI account for 42% of the total homes. Wildland fires in Southern California spreading through WUI areas in 2003 resulted in $US 2000 million of estimated insured losses (GAO 2005). Homes at risk to WUI fires are also located in Arizona, Colorado, Georgia, New Mexico, New York, and Florida (Zicherman 2004).

The most commonly used operational models for wildland fire spread rely on empirically derived relations to predict the spread rate of a fire and quantities derived from the spread rate. Examples of such models are BehavePlus (Andrews *et al.* 2003; program available at http://fire.org, accessed October

 10.1071/WF06002 1049-8001/07/010001

2006) and FARSITE (Finney 1998) in the United States, the Forest Service Fire Behaviour Prediction System (Hirsch 1996) in Canada, and the Mk 4 MacArthur Fire Danger Meters (Noble *et al.* 1980) and the CSIRO Grassland Fire Spread Meter in Australia. The essence of these models is that the local fire-spread rate is prescribed as a function of wind speed, terrain slope, humidity, and fuel characteristics. No account is taken, except for tuning the coefficients, for the fire–fuel and fire–atmosphere interactions. The data used to derive the empirical correlations employed in these models were taken either directly from field experiments and observations (Noble *et al.* 1980; Hirsch 1996) or from laboratory-scale experiments with a flat flame front with a quasi-steady spread rate across spatially homogeneous surface fuels on flat beds without a wind (Rothermel 1972; Albini 1976). Spread rates used in BehavePlus and FARSITE are based on semi-empirical relations developed by Rothermel (1972). Such models provide fire spread predictions quickly and can be easily applied to conditions that are outside those in the laboratory, sometimes with non-physical results (Beer 1991). They are also unable to predict fire behaviour in the intermix of vegetative and structural fuels that comprise the WUI.

As discussed by Finney (1998), FARSITE is unable to predict the transient behaviour of a fire due to changes in the local environment induced by the fire itself (e.g. fire–atmosphere interaction). This is because the fire shape, size, and spread rate are assumed constant for a given fuel, wind, and slope. The prediction of local wind and the interaction of the fire and wind is of major importance to predicting fire behaviour, especially severe fire behaviour (Albini 1993). Fires where strong fire–atmosphere interactions occur, such as crown fires, routinely strain the credibility of the empirical fire-spread models.

Development of these models began in the 1970s. At that time computational resources and numerical methods were not sufficiently advanced to allow three-dimensional, time-dependent simulations of wildland fires. With the dramatic increase in the capability of computers and numerical approaches in the last 30 years, population growth in WUI areas, and the increased role of prescribed burns in forest management, there is an opportunity and a need for more capable physics-based fire models. Suitably validated physics-based models for wildland and WUI fires, which predict both fire spread and smoke transport, have a number of applications:

- evaluate operational models over a wide range of relevant conditions;
- provide more realistic sources of heat and smoke for the new generation of regional smoke transport models operating on present day computational platforms (e.g. USFS BlueSky 2004);
- help land and smoke managers plan and evaluate prescribed burns;
- assess the effects of fire on vegetation during prescribed burns;
- assess how fuel treatments influence fire spread and the resulting fire effects on vegetation;
- provide a means by which established communities or homeowners can assess and/or reduce their risk to WUI fires;
- help plan firewise communities by both reducing the risk from fire spread and planning smoke-free evacuation routes; and

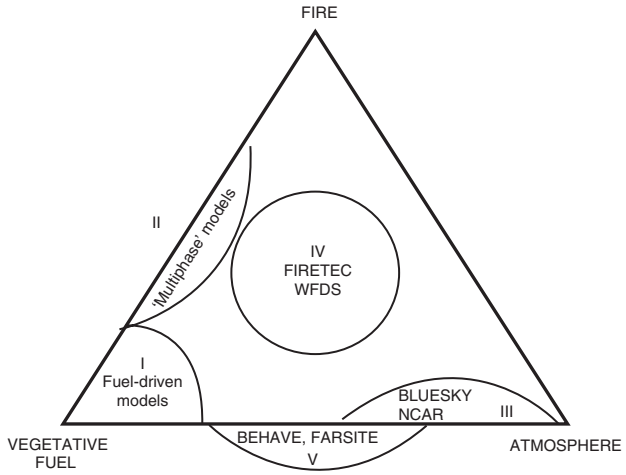

Fig. 1. The relationship of different wildland fire models. Each approach is located according to its emphasis on the atmosphere, vegetative fuel, and/or fire component(s) of the working model.

- deliver predictions of fire spread and smoke transport to incident managers to aid their management of fire fighting and evacuation logistics.

In general, simulations of wildfires require models for both the fire–fuel interaction and the fire–atmosphere interaction. The fire–fuel interaction involves gas generation by solid fuel pyrolysis, the subsequent combustion of the fuel gases, and the resulting heat flux back to the solid fuel, driving continued pyrolysis and fire spread. The fire–atmosphere interaction involves the response of both the fire and its plume to the ambient winds, and the response of the atmosphere to the buoyant fire plume. The fire–atmosphere interaction can alter the orientation and geometry of the fire plume, influencing the distribution and intensity of the net heat flux to the solid fuel, and the downwind transport of firebrands and smoke. At larger spatial and temporal scales, the interaction of the fire plume with the atmosphere can result in macroscopic (on the scale of the fire front) atmospheric processes such as pyrocumulus formation. At even larger scales, diurnal cycles in humidity and temperature, and synoptic weather patterns, can influence the behaviour of the fire and its smoke plume.

Fig. 1 is a schematic showing the atmosphere, fire, and vegetative fuel components of wildland fire models at the corners of a triangle. Different fire models are located on the figure according to the emphasis they place on each of these three components and their interaction. The Canadian FBPS (Hirsch 1996), the Australian McArthur meters (Noble *et al.* 1980), and the United States' FARSITE (Finney 1998) and BEHAVE (Andrews 1986; Andrews *et al.* 2003) models are all located in region V since these are empirical or semi-empirical, not physics-based, fire models and they require only inputs describing the vegetative fuel, terrain, and wind.

The focus of this paper is on modelling solid fuel pyrolysis, heat transfer, gas phase combustion (i.e. the fire–fuel interaction), and local fire–atmosphere interaction. A fuller investigation of large-scale fire–atmosphere interactions described above, along with firebrand generation and transport, will be considered later. In this paper the overall modelling approach is broken

into two components: (1) the pyrolysis of vegetative fuels; and (2) gas-phase combustion. Models for each are implemented within the Fire Dynamics Simulator (FDS) developed at the Building and Fire Research Laboratory at the National Institute of Standards and Technology (NIST) (McGrattan 2004) over the last 30 years. FDS numerically solves a form of the Navier–Stokes equations appropriate for low-speed, thermally driven flow with an emphasis on smoke and heat transport from fires. It is aimed at solving practical fire protection engineering problems (i.e. fires in structures) while providing a tool to study fundamental fire dynamics and combustion. Simulations can be run on single or multiple processors on most modern computer platforms. The version of FDS used here is extended to include fire spread in vegetative fuels and is referred to as WFDS (WUI Fire Dynamics Simulator).

In this paper the development of the current version of WFDS is described and evaluated by comparing its predictions of fire behaviour to open grassland fire experiments conducted by CSIRO in Australia (Cheney *et al.* 1993; Cheney and Gould 1995). The relatively simple scenario of grassland surface fires provides an appropriate first step to evaluating WFDS because the fuels are, to a good approximation, thermally thin, spatially homogeneous, occur on flat terrain, and fire spread is mostly restricted to horizontal directions (i.e. there is relatively little upward fire spread as can occur in suspended vegetation such as large tree crowns).

Review of physics-based wildland fire models

Fire models can be classified into three types (Pastor *et al.* 2003): empirical, semi-empirical, or theoretical. Empirical models involve no physics-based modelling as they are derived from statistical correlations of a given experimental dataset. Semi-empirical models are based on energy conservation but do not distinguish between the different modes of heat transfer (conductive, convective, radiative). Theoretical models attempt to solve (in some approximation) the equations governing fluid dynamics, combustion, and heat transfer. Here we refer to theoretical models as physics-based models because the physical processes governing the hydrodynamics, combustion, and energy transfer are modelled. Vegetative fuels and fires in a wildland setting are categorised as ground, surface, or crown types (see e.g. chapter 4 in Johnson and Miayanishi 2001). Examples of fuels in surface fires include fallen twigs, leaves, bark, branches, grasses, and shrubs less than 1.8 m tall (Davis 1959).

As discussed in the previous section, a complete physics-based wildland fire simulation would include models of the fire–atmosphere and the fire–fuel interactions. In this section a short overview of existing physics-based models that can be applied to surface fires is given. Fig. 1 is used to order the discussion. Note that some approaches are formulated to include a wide range of physics but then implemented in a simpler, reduced form. This is true of the approach formulated by Sero-Guillaume and Margerit (2002), and then implemented by Margerit and Sero-Guillaume (2002). Such cases are placed on Fig. 1 based on the version of the model that was implemented.

Over the last 60 years, starting with Fons (1946), many physics-based fire–fuel models for a fire spreading along a spatially homogeneous fuel bed have been presented. Examples are Albini (1985), De Mestre *et al.* (1989), Margerit and Sero-Guillaume (2002). Weber (1991) provides an excellent review of these (and other) models up to about 1989. In these approaches the fire–atmosphere interaction is not modelled. Relevant flame properties, such as the temperature and flame geometry, and therefore the heat flux from the fire, are fixed. This removes the need for modelling the fire in the fire–fuel interaction. While these models have slope and wind inputs, their physical modelling is focused on heat transfer within the fuel. For this reason they are designated 'fuel driven' models on Fig. 1 and located in region I, where modelling of the fire and atmosphere physics is less emphasised. The basis of most of these models is that the steady flame spread rate is determined by how long it takes the solid fuel ahead of the flame to reach an ignition temperature at an idealised two-dimensional ignition interface. Such models are useful for exploring the relative contributions of the different modes of heat transfer but only for conditions appropriate for steady flame spread where net wind speed and direction, fuel properties, terrain, etc., are all constant.

More recently, multidimensional, transient wildfire simulation approaches that use the methods of computational fluid dynamics to include the fire–atmosphere interaction, to varying degrees of complexity, have been developed. These methods are grouped in regions II–IV.

Region II has been labelled 'multiphase' models by most of the authors using this approach, which was first presented by Larini *et al.* (1998) and subsequently used by Porterie *et al.* (2000), Zhou and Pereira (2000), Morvan and Dupuy (2001, 2004), Morvan *et al.* (2002*a*, 2002*b*), and Dupuy and Morvan (2005) for flame spread through forest fuels. These models will be denoted MMs, for multiphase models, in the following text. While the formulation of the MMs is three-dimensional, to date all MM studies have been implemented on two-dimensional grids. The largest reported computational domain size is 200 m wide and 50 m high; 200 s of simulated time required between 12 and 48 cpu hours on a single (2 GHz) processor (Dupuy and Morvan 2005). Because the MM results have been to date two-dimensional, the complete fire–atmosphere interaction was not captured. For this reason they are placed along the vegetative fuel–fire boundary in Fig. 1. However, two-dimensionality allows relatively fine computational grids to be used and, therefore, more complete models for the thermal degradation of the vegetative fuel, the subsequent combustion of pyrolysis vapours, and the local two-dimensional fire–atmosphere interaction. The computational cost due to the complexity of the physical models limits the application of the approach to medium-scale line fires (Morvan and Dupuy 2004).

Characteristic of the MMs in region II is that of Morvan and Dupuy (2004). They model fire spread through a vegetation complex consisting of thermally thin shrubs, twigs, and grass. The solid fuel is approximated as a set of fixed fuel elements. The thermal (convective heat flux) and drag interaction of the solid fuel with the gaseous flow is accounted for by using coefficients from empirical correlations for representative shapes (cylinders, spheres, etc.). Moisture evaporation and pyrolysis are modelled with simplified temperature-dependent mass loss rates. Arrhenius kinetics are used for char oxidation. Gas-phase combustion kinetics are assumed to be infinitely fast, relative to the mixing of reactants, and the eddy dissipation model is used to determine gas-phase reaction rates. Thermal radiation in a

multiphase medium (where the volume fraction of solid versus gas is accounted for) is solved with a Discrete Ordinates solver that accounts for thermal radiation transfer within the vegetation fuel complex. An evolution equation for the soot volume fraction is solved, and a renormalisation group (RNG) k–ε turbulence model is used. Minimum grid resolutions in the fuel bed were $\Delta x = 0.1$ m, $\Delta z = 0.03$ m.

Region II also includes the simulations of Grishin and collaborators (e.g. Grishin *et al.* 1985; Grishin 1996). The formulation of the model equations is very general, including solid pyrolysis, gas-phase chemistry, and thermal radiation. However, it is unclear how these models are implemented and whether or not the reported simulation results, which span a 23-m long by 15-m high domain, are two- or three-dimensional (Grishin 1996). A k–ε turbulence model and P1 approximation for thermal radiation were used.

The methods in region III include those developed by Costa *et al.* (1995), Clark *et al.* (1996, 2003, 2004), and Coen (2003), all of which obtain the heat and moisture release, fuel consumption, and fire spread rate from either a prescribed formula or semi-empirical relations. For this reason, computational resources can be devoted to resolving atmospheric physics. For example, in the approach of Clark and colleagues (which is denoted by NCAR on Fig. 1 because its development began at the National Center for Atmospheric Research in the USA), a time-dependent three-dimensional, non-hydrostatic, cloud-resolving numerical prediction model for the atmosphere is used. The cloud-resolving model can include vertically stretched and terrain-following coordinates, and multilevel grid nesting. A recently reported application of this approach is Coen (2005). Fire spread rates are obtained from the semi-empirical Rothermel (1972) formulas. Sensible and latent heats from the fire are distributed vertically with an exponential decay over an assumed height. These approaches provide a first approximation to the fire–atmosphere coupling, especially suitable to large-scale simulations on coarse grids (from a combustion physics point of view). In Fig. 1 BlueSky refers to the modelling framework developed by the US Forest Service for smoke transport from forest, agricultural, and range fires across regional scales (USFS BlueSky 2004).

Region IV includes three-dimensional simulations that have physics-based models for the vegetative fuel, the atmosphere, and the fire. Linn and colleagues have developed a model called FIRETEC (Linn 1997; Linn *et al.* 2002; Linn and Cunningham 2005). FIRETEC was designed to operate over landscape scales (100s of metres) of flat or complex terrain. The three-dimensional nature of the model and its focus on the coupling between the atmosphere and fire constrain the ability of this model to use far sub-meter resolution over domains more than 300 m in all directions (R. R. Linn, personal communication 2005). Thus, the fine-scale turbulence and combustion processes cannot be resolved directly and must be approximated with subgrid models. In fact, any three-dimensional simulation, run on present day computational platforms, of full-scale fires requires subgrid models (including WFDS).

The governing model equations in FIRETEC are based on ensemble averaging, in a manner similar to Reynolds averaging, of the conservation equations for mass, momentum, energy, and chemical species. This results in additional closure equations, which require a number of turbulence modelling assumptions. FIRETEC is coupled to an atmospheric model HIGRAD (Reisner *et al.* 2000). A numerical time stepping scheme explicitly handles the high-frequency acoustic waves. Thermal radiation transfer is computed using a diffusional transport approximation adapted from Stephens (1984). The chemical heat release from combustion occurs only in computational grid cells that contain the solid fuel (Linn *et al.* 2002). For grid cell dimensions that are smaller than the flame length this is unrealistic and improvements are underway (Colman and Linn 2003, 2005). A heat-release rate is determined from a universal reaction rate that is a function of the density of both the solid fuel and the gas phase, and an assumed Gaussian-shaped probability density function (PDF) of the temperature within a grid cell. The use of this PDF is physically motivated by the assumption that in general there are wide variations in temperature within a grid cell that are not sufficiently represented by the resolved temperature. The heat-release rate, determined from the universal reaction rate and a heat of combustion of the volatiles, is partitioned between the gas and the solid (Linn *et al.* 2002). In both the gas- and the solid-phase energy equations these terms are exothermic. A weight factor is applied to these exothermic terms. In the solid-phase energy equation the weight factor increases as the solid burns away; in the gas-phase energy equation the weight factor has the opposite trend. For example, the weight factor that determines how much energy is returned to the solid fuel ranges from 25 to 75%; the highest value is applied when oxygen is abundant and more than 60% of the solid fuel mass is gone (R. R. Linn, personal communication 2005). The motivation for this approach is to account for the progression from flaming to non-flaming combustion and to model the unresolved subgrid heat transfer processes in the vicinity of the fire.

Compared to the MM approach (which more directly solves the governing equations on more highly resolved two-dimensional computational grids) FIRETEC currently relies more on heuristic, physically motivated assumptions, such as a prescribed subgrid probability distribution of the temperature in a grid cell and a rule for partitioning the energy release rate into the gas and solid phases. Many of these assumptions are driven by the limitations on spatial resolution in FIRETEC.

Overview of WFDS modelling approach

This section is an overview of the WFDS modelling approach. A detailed description of the model equations for the gas phase and vegetative fuel is given as an Accessory Publication on the *International Journal of Wildland Fire* website. The approach is similar to the MM approach described above (e.g. Porterie *et al.* 1998) because separate but coupled models for the thermal degradation of the solid fuel and gas-phase combustion are employed. This allows for a straightforward use of some of the physics-based solid-phase models (region I of Fig. 1). As discussed above, these fuel-driven models use an assumed flame geometry and temperature. Thus, in place of a constant heat flux on the solid fuel from an assumed flame, a transient heat flux (both convective and radiative) is used. This heat flux results from the local fire–atmosphere interaction as determined by the numerical solution of the conservation equations for momentum, total mass, energy, and the major species. Combustion is modelled with a mixture fraction-based approach.

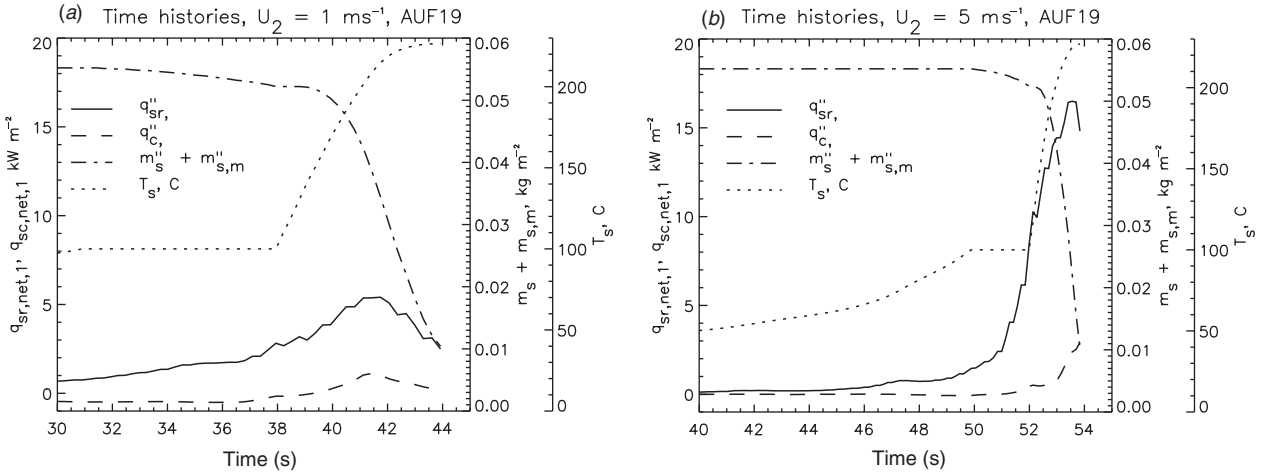

Fig. 2. Time history of quantities in the uppermost layer of the grassland fuel model for two different ambient wind speeds at 2 m above ground. (*a*) $U_2 = 1\,\mathrm{m\,s^{-1}}$; (*b*) $U_2 = 5\,\mathrm{m\,s^{-1}}$. In each the following are plotted: the convective ($\dot{q}''_c$) and net radiative ($\dot{q}''_{sr}$) fluxes on the top of the layer and the temperature (T, in °C) and net mass loading (dry and moisture mass, $m''_s + m''_{s,m}$) of the layer.

Unlike the MM approach, which is limited to two-dimensional grids, WFDS can simulate fires in two or three dimensions (only fully three-dimensional simulations, with no symmetry assumptions, are reported here). Since three-dimensional simulations require significantly more computational resources, WFDS grids are coarser than those used in the MM approach. As a result, a combustion modelling approach appropriate for computational grids that significantly under-resolve the combustion zone must be used. The approach used here is described in the Accessory Publication. Compared to FIRETEC, which also operates on coarse grids (relative to the MM approach), WFDS more directly solves the equations governing the fire–fuel and fire–atmosphere interactions, relying less on heuristic physically motivated assumptions to include physical processes. For example, the thermal degradation of the solid fuel is driven solely by the resolved net heat flux on the fuel. In FIRETEC an additional amount of energy, a fraction of heat released by a combined solid–gas reaction, is deposited in the solid fuel (Linn and Cunningham 2005).

The basis of the surface vegetation model in WFDS is the physical assumption that combustion (i.e. heat release) occurs predominantly above the surface fuel bed. This is consistent with flame heights above the fuel bed that are significantly larger than the height of the fuel bed itself. With this assumption, two computational grids can be used – one for the gas phase that resolves the fire plume and another for the vegetative fuel bed that resolves heat transfer and thermal degradation. The fire plume can be resolved on a much coarser grid than the thermal degradation of the vegetation. The equations solved and numerical method employed in the gas-phase calculation are essentially those used by McGrattan (2004); details are in the Accessory Publication. The vegetation is 'seen' by the gas phase as a source of momentum drag and heat and mass fluxes along the bottom boundary of the gas phase. Heat flux (from the fire) and fuel gas flux (from pyrolysis) both occur along the upper boundary of the grid for the vegetative fuel bed. A method that is similar to the multiphase approach discussed previously is then used to model the evolution of solid phase. Gas-phase temperatures in the fuel bed are obtained from the gas-phase computational grid directly above. The approach is described in more detail in the Accessory Publication. Note that this approach is less valid for vegetative fuels through which significant vertical flame spread and air flow can occur (such as through tree crowns). For the Australian grassland fire experiments simulated here the observed flame heights above the fuel bed were about four times the height of the fuel bed. An alternative modelling approach for raised fuels has been developed and is being validated. Preliminary results from this approach can be found in Mell *et al*. (2007).

Fig. 2 shows the time history of a number of solid-phase quantities, in the uppermost layer of the solid fuel model, for wind speeds U_2 of 1 and $5\,\mathrm{m\,s^{-1}}$, where U_2 is the wind speed 2 m above the ground. The grassland fuel properties measured in experiment F19 conducted in Australia were used (see Table 1; details of this experiment are given in section 'Case studies'). The time interval in each plot is 15 s. In the slower wind case (Fig. 2*a*) 15 s is the time required for evaporation of the fuel moisture ($T_s = 100$ C) and the subsequent pyrolysis of the solid fuel (leaving only char). At this point in its development, the model does not account for char oxidation (smouldering combustion). In Fig. 2*b* boiling and pyrolysis occur over a shorter time interval of 4 s, due to the higher heat fluxes on the solid fuel. The peak heat fluxes are over a factor of two larger in the faster wind case. The faster wind forces both the flame and the hot fire plume closer to the downwind fuel bed, increasing both the radiative and convective heat fluxes. This is a well-known process leading to faster fire spread in stronger winds. For both wind speeds, radiation is the dominant heat-transfer mechanism. In the simulations of Morvan and Dupuy (2004) the relevance of convective heat transfer was found to increase with increasing wind speed, eventually becoming the dominant mode of heat transfer. Their two-dimensional simulations use significantly smaller gas-phase grid cells (O(10) cm compared to O(1) m) resulting in much higher, and more realistic, gas-phase temperatures in the fire plume. As a result, convective heat

transfer into the solid fuel in regions of active combustion are underestimated in WFDS. This is an area of further model development. However, as will be seen below, WFDS does reproduce many experimentally observed fire spread trends.

Results

Overview of grassland fire experiments

Experiments were conducted on a 2500 ha (25×10^6 m^2) site in the Northern Territory of Australia, during July and August 1986 (Cheney *et al.* 1993; Cheney and Gould 1995). Fuels were open grasslands, and grasses were continuous and normally fully cured. The site was divided into 170 plots that were 100 × 100 m, 200 × 200 m, or 200 × 300 m in size. A total of 121 of these grassland fires was used by Cheney *et al.* (1993) to examine the influence of fuel and wind on the spread rate of the head fire, R. Each fire travelled over flat terrain.

Plots contained one of two distinct grass types: *Eriachne burkittii* (kerosene grass), a coarser grass with a mean surface area-to-volume ratio of 9770 m^{-1}; and *Themeda australis* (kangaroo grass), a finer grass with a mean surface area-to-volume ratio of 12 240 m^{-1}. Selected plots were harvested to alter the height, h_s, load, w_s, and bulk density, ρ_{sb}, of the fuel. Plots were either natural or cut at 25–50% of natural grass height. The cut fuels either remained or were removed. Characteristic h_s, w_s, and ρ_{sb} values were determined for each plot, and only plots with fairly even fuel load and continuous fuels were included in the analysis. Moisture content of the grass fuel, M, as a fraction of the oven-dried weight of the grass was measured (expressed as a percentage).

Wind speeds at 10 m and 2 m above ground level (AGL) were measured in the open area immediately upwind and within 800 m of each fire. Wind speeds at 2 m AGL at each corner of the experimental plot were also measured at 5-s intervals for the duration of the fire. Wind orientation was not measured, only the speed of the horizontal wind. Ignition, by field workers carrying drip torches, started at the mid-point of a measured line and moved rapidly toward each end along the upwind edge of the grass plot. Thus, the fire could not spread upwind. Ignition lines were nominally 50 m long on 100 × 100 m plots, and up to 175 m long on the larger plots. Ignition line fires were oriented at right angles to the prevailing wind direction. The average forward rate of spread, R, was determined over the longest period of spread before a substantial change in the rate of spread.

Overview of the numerical simulations

A number of simulations, with ignition line-fires of varying length, L_{ig}, depth, d_{ig}, and wind speed 2 m above the ground, U_2, were conducted to assess how well WFDS predicts the spread rate of the head fire. Two additional simulations, of specific Australian grassland experiments (F18 and C064; Table 1), were run to evaluate WFDS predictions of the behaviour of the entire fire perimeter.

The physical parameters required by the model are listed in Table 1 for both the gas phase and the vegetative fuel. Whenever possible, values obtained from the grass fire experiments are used. Properties that were not measured in the field were determined from literature sources for similar conditions (see Table 1). All boundaries except the inflow and bottom are open. At the open boundaries the density and mixture fraction have zero gradient conditions; velocity and pressure boundary conditions are described in McGrattan (2004).

Initially, throughout the domain and at the inflow boundary for the duration of the simulation, the dependence of the ambient wind with height above the ground, z, is defined to follow a power law:

$$U(z) = U_{2,i}(z/2)^{1/7}. \quad (1)$$

Here $U_{2,i}$ is the value in WFDS of the initial wind speed at a height of 2 m. This expression is suitable for smooth terrain

Table 1. Thermophysical properties required in model and values used in base case simulations

Properties that were not measured in the two experimental field studies F19 or C064 are denoted by a dash. Values of these unknown properties in the simulation were either assumed or representative values were obtained from the literature sources cited. See Appendix 1 for definition of variables

Phase	Symbol, units	Value used	F19	C064	Other source (if needed)
Gas	Δh_c (kJ kg^{-1})	15 600	–	–	Grass (Hough 1969; Susott 1982)[A]
	χ_r	0.35	–	–	Wood cribs (Quintiere 1997)[A]
	χ_s	0.02	–	–	Douglas fir (Bankston *et al.* 1981)[A]
	dT_a/dz (°C m^{-1})	0.0	–	–	Assumed
	U_2 (m s^{-1})	Experimental	4.8	4.6	
	$T_{g,a}$ (°C)	Experimental	34	32	
Solid	σ_s (m^{-1})	Experimental	12 240	9770	
	χ_{char}	0.2	–	–	Grass (Susott 1982)[A]
	$c_{p,v}$ (kJ kg^{-1} °C^{-1})	Varies with T_s	–	–	$= 1.11 + 0.0037T_s$ (Parker 1989)
	$c_{p,m}$ (kJ kg^{-1} °C^{-1})	4.22	–	–	Incropera and Dewitt (1996)
	h_s (m)	Experimental	0.51	0.21	
	ρ_s (kg m^{-3})	512	–	–	Grass (Rothermel 1972)
	w_s (kg m^{-2})	Experimental	0.313	0.283	
	β_s	Experimental	0.0012	0.0026	
	M (%)	Experimental	5.8	6.3	
	Δh_{pyr} (kJ kg^{-1})	416	–	–	See discussion in Accessory Publication
	$T_{s,a}$ (°C)	$T_{g,a}$	–	–	Assumed

[A]Representative value from range of values found in the cited reference.

and has been used in simulations of fire spread in pine needle beds (Morvan and Dupuy 2001) and in a grass/shrub fuel bed (Morvan and Dupuy 2004). Other ambient wind profiles can easily be implemented but their influence on simulated fire behaviour will be investigated elsewhere (e.g. Mell *et al.* 2005). In general, U_2 can be modified by drag from surface vegetation and the fire plume (due to both entrainment and blockage effects). When comparing head fire spread rates from WFDS and the experiments over a range of conditions a consistent measure of the representative ambient wind speed U_2 must be used. The experimental value of U_2 was determined by averaging, over the time interval spanning ignition to when the fire reached the downwind firebreak, the measured horizontal wind speed at the two upwind corners of the plot (see Fig. 3). The simulated value of U_2 was determined by averaging, over the same time interval used to compute the experimental U_2, the horizontal wind speed in the grid cell located at the center of the ignition line fire and at a height of $z \cong 2$ m. For the simulations reported here this velocity location was within a height range of $z = 1.95$ m to 2.1 m. The magnitude of the crosswind velocity, v, in WFDS was initially zero and remained much smaller than u so that $(u^2 + v^2)^{1/2} \cong u$. The corner values of the simulated velocity were not used to define U_2 in the simulations because they were not representative (they were too low due to drag from unburned vegetation) of the wind speed upwind of the head fire.

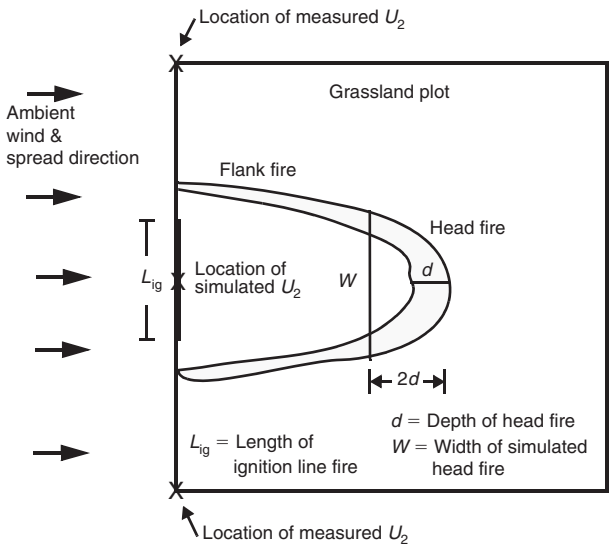

Fig. 3. A schematic of a grassland fire. The ambient wind flows from left to right. The value of the wind speed, U_2, in the experiments is obtained by averaging the magnitude of the horizontal velocity measured at a height of $z = 2$ m positioned at the upper and lower left-hand-side corners of the grassland plot. The value of the wind speed in the simulation is obtained from the computed component of the velocity vector parallel to the ambient wind at a height of $z \cong 2$ m positioned above the center of the ignition line fire.

The heat release rate per unit area of an ignition line fire has two components: the burning grass and the hydrocarbon fuel deposited by the drip torches. The hydrocarbon fuel was assumed to be gasoline (heat of combustion 32 MJ L^{-1}) deposited with an area density of 0.25 L m^{-2}. Complete burning of the gasoline and grass fuel was assumed to occur over a time interval equal to d_{ig}/R_{ig} where $R_{ig} = 0.3$ m s^{-1} is assumed (based on experimental head fire spread rates). For example, in simulations using the grassland fuel present in experiment F19 (see Table 1) an ignition line fire of depth $d_{ig} = 3.3$ m had a duration of 11 s and a heat release rate per area of 1460 kJ m^{-2}. The ignition procedure, which can be easily modified, will affect the initial behaviour of the fire. Since the information available for the field ignition method was incomplete (e.g. it is unknown how much liquid fuel was distributed on the grass) the method used here is a best estimate to the field procedure.

Care must be taken to avoid nonphysical numerical boundary affects. A fire entrains the surrounding ambient air into its rising plume. The numerical boundaries must not interfere with this process in a significant way. For example, when the inflow boundary (at which the wind speed is held fixed) is too close to the fire, entrainment from the upwind direction is reduced. This can have significant effects for sufficiently low ambient wind speeds. In reality, under such conditions entrainment by a fire plume in an unbounded domain can add to the ambient wind oriented into the head fire. In numerical simulations with upwind boundaries that are too close to the fire, the flame spread rate increases as the boundary is moved further from the fire.

It was found that spread rates and fire behaviour were nearly identical when the grassland plot was centered in a 1500 m versus a 2700 m square domain. In the simulations discussed below, therefore, the fires occurred within a 300×300 m plot surrounded by a 600 m border on all sides (1500×1500 m area). A number of tests were made to check the influence of grid resolution on head fire spread rates. In these tests the sizes of horizontal grid cells were $\Delta x = \Delta y = 1$ m, 1.66 m, or about 3.33 m. As the grid resolution increased, the head fire spread rate decreased

Table 2. Simulation parameters for production runs

The horizontal grid cell sizes are equal $\Delta x = \Delta y$. The values of Δx given in the table are for a 300×300 m region in the center of the overall simulation domain. Outside this central region the horizontal grid cells are twice this size. The vertical grid size increases upward (72 grid cells are used). Each simulation required sixteen million grid cells and 11 processors. Processor speed was 1.8 GHz. Case F19 required 44 cpu hours for 100 s of simulated time. Case C064 required 25 cpu hours for 100 s of simulated time. Case C064 required less resources because the overall heat release rate was approximately half that of case F19, resulting in smaller buoyancy induced velocities and, therefore, larger time steps

Simulation	U_2 (m s^{-1})	L_{ig} (m)	d_{ig} (m)	Fuel bed	Grass plot x,y extent (m × m)	Simulated domain extent (m × m × m)	Δx, Δz (m)
Head spread	1, 3, 4, 5	8, 25, 50, 100	6.7, 6.7, 3.3, 3.3	= Exp F19	200 × 200	1500 × 1500 × 200	1.6; 1.4 → 5.5
Exp F19	4.9	175	3.3	see Table 1	200 × 200	1500 × 1500 × 200	1.6; 1.4 → 5.5
Exp C064	4.6	50	1.6	see Table 1	104 × 108	1500 × 1500 × 80	1.6; 0.6 → 5.5

somewhat. Spread rates with the $\Delta x = 1$ m were 15% (or less) slower than the $\Delta x = 3.33$ m cases and 10% (or less) slower than $\Delta x = 1.66$ m cases. Table 2 contains the values for grid resolution and other parameters for the production simulation runs.

Production simulations ($1500 \times 1500 \times 200$ m, in general) required 16×10^6 grid cells and 11 processors. The total cpu time required for these runs depended on the overall heat release, which increases with fuel loading. For most of the cases considered 44 cpu hours were needed for 100 s simulated time (i.e. all 11 processors running for 44 h on 1.8 GHz processors). Exploratory simulations run much faster, on the order of 2 h on a single processor. These faster runs were on smaller domains and provide reasonable results if the ambient wind speed is sufficiently high. For lower ambient wind speeds ($O(1)$ m s^{-1}) natural entrainment was influenced by the presence of numerical boundaries as discussed above. Thus, for consistency all simulations had horizontal domains of 1500×1500 m.

It should be noted that the results of any large-scale simulation will depend on both the grid resolution and the modelling assumptions employed. Fully resolving the combustion zone (as captured by the relatively simple fast-chemistry mixture fraction approximation used here) requires sub-millimeter grid resolution (Mell *et al.* 1996). The larger-scale fire–fuel interactions, which control the heat transfer to the fire bed, occur on scales on the order of 1–10 m for grass fires, a factor of over a thousand greater. Fire–atmosphere interactions occur over even larger scales. Present day computers (even massively parallel platforms containing thousands of processors) do not have the memory capacity or processor speeds to fully resolve processes occurring from the combustion zone up to scales that characterise the fire–atmosphere interactions. For this reason, the governing equations must be approximated in a way that retains the physical processes that are most relevant to the fire problems under study. Here the emphasis is placed on resolving the larger-scale fire plume dynamics and heat transfer processes, in the fire–fuel and fire–atmosphere interactions, that drive fire spread (as opposed to smaller scale combustion processes of, for example, chemical kinetics and soot generation). In the following sections WFDS will be evaluated by determining how well it reproduces observed fire-spread trends in the Australian grassland experiments.

A characteristic example of both the experiment and simulation is shown in Fig. 4. A photograph of the fire perimeter taken during experiment F19 is shown in Fig. 4*a*. A rendering of the simulated fire front and smoke plume using the visualisation tool Smokeview (Forney and McGrattan 2004) is plotted in Fig. 4*b*. As discussed above, smouldering combustion is not currently modelled. For this reason, there is no smoke generated upwind of the fire in the simulation (Fig. 4*b*).

Effect of wind on head fire spread

Cheney *et al.* (1993) found that when head fire spread rate was correlated with fuel type, wind speed, and fireshape variables, wind speed U_2 had the most effect on the spread rate. Convective activity was thought to be a primary factor that determined whether fires progressed steadily in the direction of the prevailing wind, and fires burning under light wind conditions often spread erratically as they responded to gust and lulls caused by the localised thermal activity. As the wind speed increased,

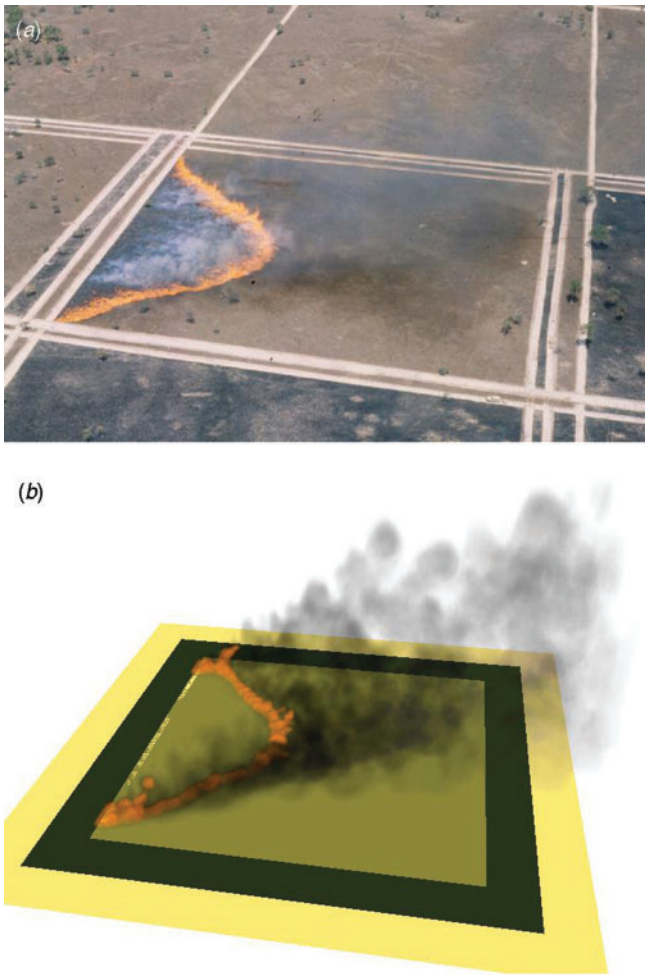

Fig. 4. (*a*) Photograph of experimental fire F19 at $t = 56$ s. (*b*) Snapshot of WFDS simulation of experimental fire F19 at $t = 56$ s.

the head fire width required for fires to approach their potential quasi-steady rate-of-forward spread, R_s, also increased. Cheney *et al.* (1993) note that the wind directly influencing fire spread is the net wind at the flame zone, not the wind measured remote from the fire. However, since this net wind speed is not known and would be very difficult to measure, empirical formulas for the spread rate of the head fire are based on a representative ambient wind U_2. The determination of U_2 was discussed above.

The following empirically based formula (eqn 4 in Cheney *et al.* 1998) relates the experimentally observed head fire spread rate, R_o, to the measured wind speed U_2, the head fire width W, and the fuel moisture content M:

$$R_o = (0.165 + 0.534U_2)\exp([-0.859 - 2.036U_2]/W)\exp(-0.108M). \quad (2)$$

They defined the head fire width, W, as the width of the fire measured at right angles to the direction of head spread, which influenced the shape and size of the head fire during the next period of spread measurement (Cheney and Gould 1995). The effective width of the head fire can also be defined as that portion of the perimeter where the flames are leaning towards unburnt fuel. In WFDS the head fire width was defined to be the distance

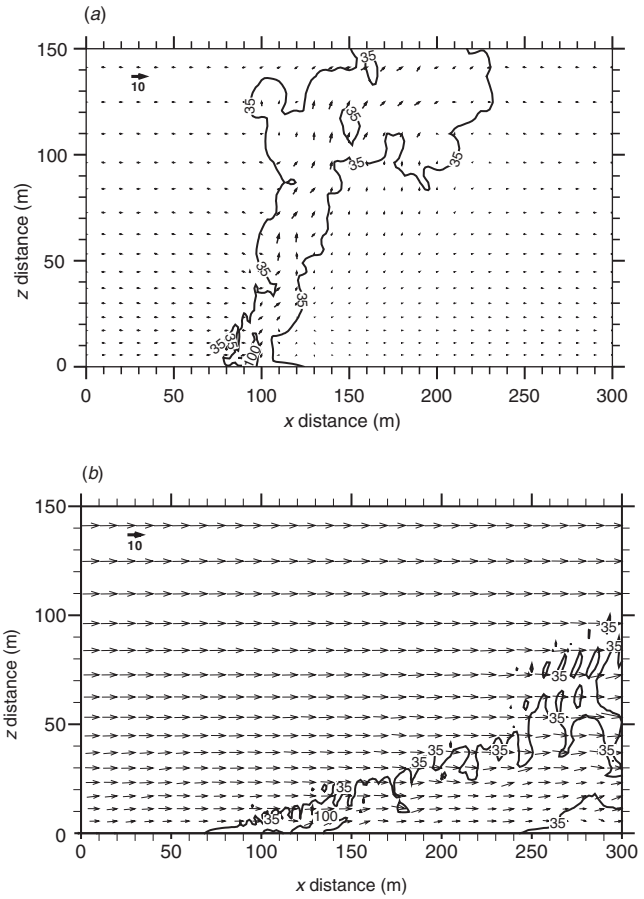

Fig. 5. Temperature contours (35 and 100°C) and velocity vectors in an *xz*-plane for fires spreading in a grassland fuel bed with the characteristics of experiment F19 (see Table 1). The length of the ignition line fire was $L_{ig} = 50$ m. The two figures correspond to two different wind speeds: (*a*) $U_2 = 1$ m s^{-1} at $t = 100$ s; (*b*) $U_2 = 5$ m s^{-1} at $t = 50$ s. Horizontal spacing of vectors is 10 m (every sixth grid cell); vertical spacing varies because the grid is stretched (every fourth cell is shown). The depth of the ignition line fire is ~7 m and is located at $x = 50$–57 m.

between the flank fires one fire depth upwind of the trailing edge of the head fire (see Fig. 3). With increasing head fire width, $W \to \infty$, the head fire spread rate, Eqn (2), increases and asymptotes to a potential quasi-steady spread rate (Cheney *et al.* 1998):

$$R_s = (0.165 + 0.534U_2)\exp(-0.108M). \quad (3)$$

In the figures to follow, simulated head fire spread rates and head fire location were compared to their experimentally observed values through the use of these empirical spread rate relations.

Simulations using four different ignition line fires, $L_{ig} = 8$, 25, 50, and 100 m, and four wind speeds, $U_2 = 1$, 3, 4, and 5 m s^{-1}, were run (16 simulations in all). See Table 2 for a summary of the simulations. For each case the line fire was ignited simultaneously along its entire length. The fuel bed parameters of experiment F19 (see Table 1) were used. The wind speeds used are such that the fire–atmosphere interaction ranges from a more plume-dominated fire to a wind-dominated fire (Pagni and Peterson 1973; Pitts 1991). Fig. 5*a* shows the more plume-dominated

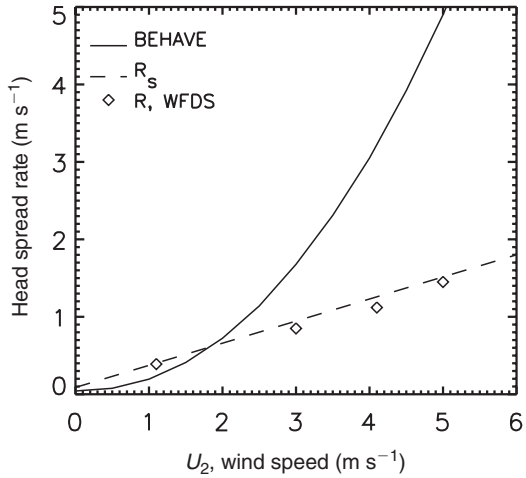

Fig. 6. Spread rate of head fire versus the wind speed at a height of 2 m. Symbols are WFDS; solid line denoted BEHAVE is from the BehavePlus computer program and dashed line is the empirical expression (Eqn 3) from the grassland fire experiments (i.e. eqn 4 in Cheney *et al.* 1998 with $W \to \infty$).

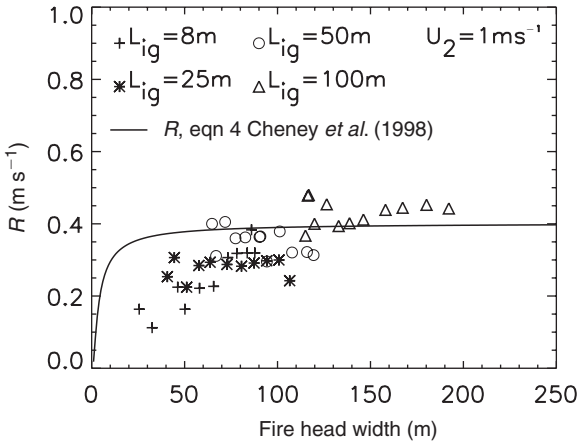

Fig. 7. Spread rate of head fire versus the width of the head fire. Wind speed $U_2 = 1$ m s^{-1}. Spread rates from four different lengths of the ignition line fire ($L_{ig} = 8$, 25, 50, and 100 m) are shown. Symbols are WFDS; solid line is determined using the empirical expression, Eqn (3), from the grassland fire experiments (eqn 4 in Cheney *et al.* 1998).

case ($U_2 = 1$ m s^{-1}). In this figure the plume rise close to the ground ($z < 20$ m) is dominated by buoyancy resulting in a nearly vertical rise. In Fig. 5*b* the wind ($U_2 = 5$ m s^{-1}) dominates the plume rise. As shown previously in Fig. 2 the net heat flux to the solid fuel is significantly higher for the faster wind speed case due to flame tilt toward the unburned fuel bed.

Fig. 6 is a plot of head fire spread rate versus wind speed. Spread rates from WFDS (symbols), BehavePlus (Andrews *et al.* 2003) (solid line), and the empirically derived quasi-steady spread rate form of Eqn (3) (i.e. $W \to \infty$) (dashed line) are shown. The spread rate from WFDS was obtained from the time history of the leading edge of the head fire. The leading edge was identified by the location of non-zero fuel mass loss rate, along the centerline of the grass plot, that was furthest downwind. As is seen above, in Fig. 7, WFDS spread rates for $L_{ig} = 50$ m quickly

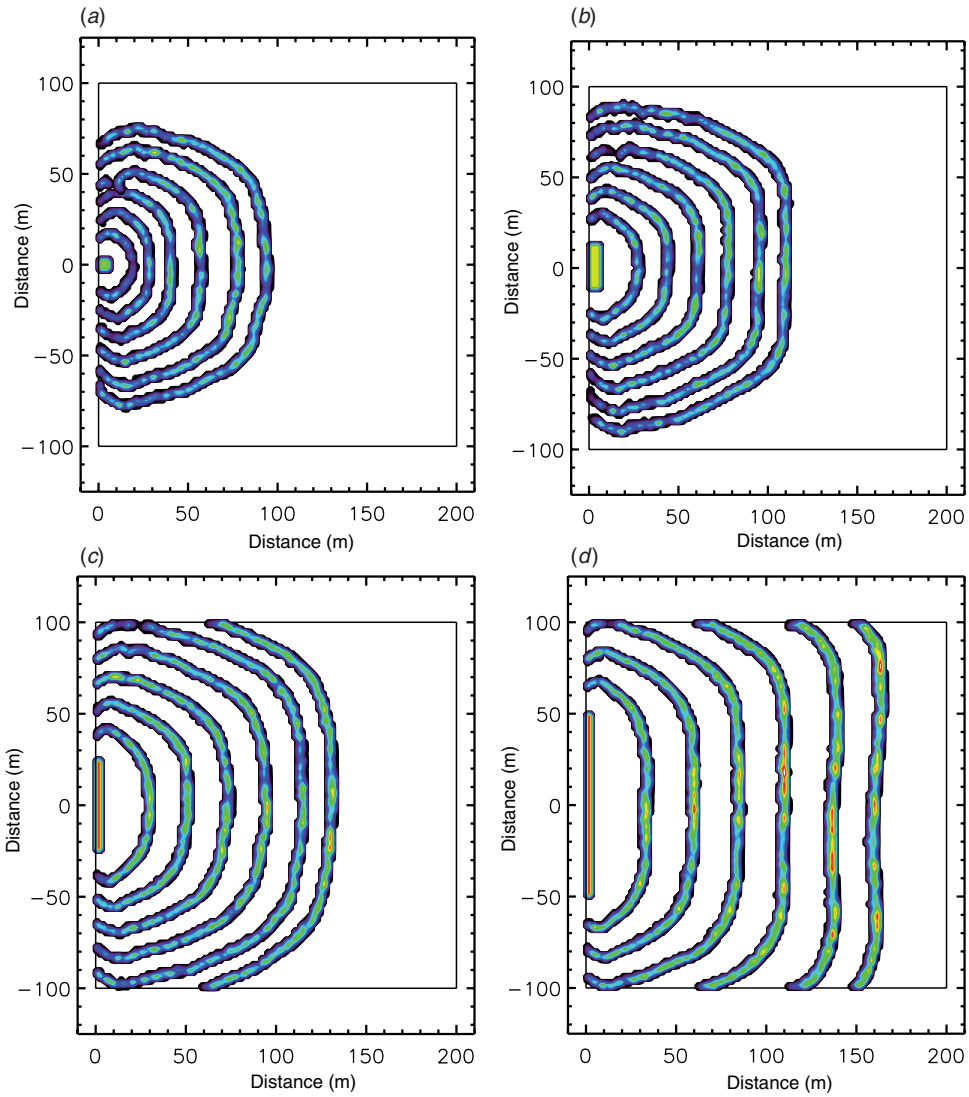

Fig. 8. Time evolution of fire perimeters, shown as shaded contours of the mass loss rate, for $U_2 = 1\,\mathrm{m\,s^{-1}}$, and four different ignition line lengths L_{ig} of (*a*) 8 m, (*b*) 25 m, (*c*) 50 m, and (*d*) 100 m. The fire perimeters are plotted at times $t = 0$, 60, 120, 180, 240, 300, and 350 s. The fire spreads in a 200 × 200 m grassland plot with the fuel properties of experiment F19 listed in Table 1.

reach a quasi-steady value. The dependence of the spread rate on the wind speed is well predicted by WFDS. The quantitative agreement of WFDS is also good, however it is important to note that the sensitivity of WFDS to realistic variations in environmental variables (wind speed, moisture content, etc.) has not yet been assessed.

Another important issue is how the value of the wind speed, U_2, is obtained. As discussed in the previous section, both Eqns (2) and (3) and the WFDS inflow boundary condition use a value of U_2 that is the average wind speed at a height of ∼2 m. In BehavePlus the default height of the wind speed is at the mid-flame height. The experimentally observed average mid-flame height, for $U_2 = 4.8\,\mathrm{m\,s^{-1}}$, was 1.3 m for this fuel and the mid-flame wind speed was $4.5\,\mathrm{m\,s^{-1}}$. With $U_2 = 4.8\,\mathrm{m\,s^{-1}}$, input in BehavePlus for the mid-flame wind speed R is $4.4\,\mathrm{m\,s^{-1}}$ (this is plotted in Fig. 6). With the observed value of $4.5\,\mathrm{m^{-1}}$ for the mid-flame wind speed input into BehavePlus R is $3.9\,\mathrm{m\,s^{-1}}$. This still significantly overpredicts the empirically determined spread rate of the head fire, which is $R = 1.4\,\mathrm{ms^{-1}}$. The overprediction of the spread rate by Behave for fuels with a surface-to-volume ratio of $13\,100\,\mathrm{m^{-1}}$, which is similar to the fuel used here ($\sigma_s = 12\,240\,\mathrm{m^{-1}}$), has been noted before (Gould 1988).

Effect of fire head width on fire spread

After U_2, the head-fire width, W, was observed to account for the greatest variation in spread rate in the grassland experiments. The correlation between R and the measured moisture content of dead grass M was not significant. This was attributed to difficulties with sampling and handling techniques for measuring M, the relatively small range of M during the experiments, and

to the large effect of wind speed masking the effect of moisture content. Cheney and Gould (1995) found that R_o, for a given U_2, rapidly increased as W increased. For lower wind speeds ($U_2 < 3.5\,\mathrm{m\,s^{-1}}$), R_o appeared to asymptote when $W \cong 50\,\mathrm{m}$. For $U_2 > 3.5\,\mathrm{m\,s^{-1}}$ both R_s and the value of W at which $R_o \approx R_s$ increased. Cheney *et al.* (1993) comment that models developed from experimental fires that have not been allowed to burn to a substantial size ($W > 100\,\mathrm{m}$) are likely to underpredict the spread rates of wildfires, particularly at higher wind speeds.

Fig. 7 shows the head fire spread rate versus the head fire width for $U_2 = 1\,\mathrm{m\,s^{-1}}$, and the four different lengths of the ignition line fire, $L_{ig} = 8$, 25, 50, and 100 m. The solid line is the spread rate from Eqn (2). The simulations reproduced the trend of an increasing head fire spread rate with an increasing width of the head fire. The head width increased monotonically with time (not shown). All ignition line length cases, with the possible exception of $L_{ig} = 8\,\mathrm{m}$, reach a quasi-steady spread rate that is within 25% of the Eqn (3) value. Longer ignition line cases reach spread rates that are closer to the Eqn (3) value (i.e. the plateau value of the solid line). The experimental fires, as described by Eqn (2), obtained a quasi-steady spread rate at narrower head fires than the simulated fires. Fig. 8*a–d* shows sequential snapshots of the burning region (shaded contours of the mass loss rate are shown) for each of the ignition line fire lengths used. Note that for the $L_{ig} = 50\,\mathrm{m}$ and 100 m cases, Fig. 8*c*, *d* respectively, the flank fires reach the upper and lower fire breaks.

In Fig. 9, results with $U_2 = 5\,\mathrm{m\,s^{-1}}$ are shown. In the left column the location of the leading edge of the head fire (solid line) versus time from WFDS is plotted. Each row in Fig. 9 corresponds to a different ignition line fire length. Also shown in the left column are the width (W, dashed line) and depth (d, dotted line) of the head fire. In each case an initial time period of relatively rapid spread is present, followed by a slower spread rate. This initial rapid spread may depend on the ignition procedure, and needs to be investigated. In order to compare to experimental fire behaviour, the location of the head fire is also determined using the empirical relation, Eqn (2) (circles). This equation is implemented using W calculated by WFDS and $U_2 = 5\,\mathrm{m^{-1}}$. For the cases with $L_{ig} = 25\,\mathrm{m}$, 50 m, and 100 m WFDS predictions of the head fire location agree well, overall, with those derived from Eqn (2). At the latest time WFDS does overpredict the location of the head fire, but by less than 8%. When $L_{ig} = 8\,\mathrm{m}$ there is an initial period of time, greater than 30 s, during which the head fire spread rate increases before reaching an more quasi-steady value after $t \cong 110\,\mathrm{s}$. The head width (dashed line) at which the simulated head fire spreads in a quasi-steady manner is approximately $W = 65\,\mathrm{m}$ (note Fig. 7 shows similar results for $U_2 = 1\,\mathrm{m\,s^{-1}}$). This is consistent with experimental observations that spread rates are relatively unaffected by L_{ig} when $L_{ig} > 75\,\mathrm{m}$ and U_2 is sufficiently small. Relatively little change in the head fire width occurs for $L_{ig} = 100\,\mathrm{m}$. Cheney and Gould (1995) note at their highest wind interval between 4.7 and 7.1 $\mathrm{m\,s^{-1}}$, a head fire width of more than 125 m in open grassland is required to get spread rates within 10% of the quasi-steady rate of spread. Thus, with an ignition line of 100 m, spread rates could still be increasing at wind speeds of $5\,\mathrm{m\,s^{-1}}$. The oscillations in the location of the head fire and fire depth (most clearly seen Fig. 9*b*) are due to interactions of the fire plume and the local wind field. Note that increases in R are associated with increases in d.

Fig. 9 (right column) shows the fire perimeter at 60 s intervals. The relatively high wind speed results in head fire depths (10–12 m) that are greater than the flank fire depths (5–7 m). This does not occur in the weak wind case ($U_2 = 1\,\mathrm{m\,s^{-1}}$, in Fig. 8). This behaviour is consistent with field observations. The average head fire depth from field measurements for $L_{ig} = 175\,\mathrm{m}$ and $U_2 = 4.8\,\mathrm{m\,s^{-1}}$ is $d = 10\,\mathrm{m}$. Observed fire depths were interpreted from oblique photographs that were rectified and plotted onto a planar map of time isopleths of fire perimeter and fire depth.

Residence time, mass flux, heat release rate

Fig. 10 is a plot of the head fire residence time, τ, versus the spread rate of the head fire. Residence times from the WFDS simulations, Australian experiments, and an empirical formula from Anderson (1969) are plotted on the figure. In the empirical formula the residence time, $\tau = d/R$, is a function only of the surface-to-volume ratio:

$$\tau = d/R = 75\,600/\sigma_s. \tag{4}$$

Sneeuwjagt and Frandsen (1977) tested Eqn (4) and state it provided a good fit to data from their grassland fire experiments. The value of τ from Eqn (4), using σ_s for the two Australian grassland experiments C064 and F19, is shown in Fig. 10 as horizontal lines labelled C064e and F19e. The value of σ_s is 9770 $\mathrm{m^{-1}}$ and 12 240 $\mathrm{m^{-1}}$ for C064e and F19e, respectively (see Table 1). The value of τ, based on measured values of d and R in the Australian experiments, are denoted by C064AU and F19AU. Symbols mark the value of τ from WFDS predictions of d and R for a range of L_{ig} and U_2 conditions with F19 grassland fuel. The value of the depth of the head fire, d, is in the direction of spread (see Fig. 3). C064s or CF19s denote WFDS results for conditions identical to the two Australian experiments. WFDS values of τ are larger than those from Eqn (4); but only weakly dependent on R (especially for the larger L_{ig} values), which is consistent with Eqn (4).

An important implication of Eqn (4) is that the mass loss rate, $\dot{m}''_s$, and therefore the reaction intensity, I_R, averaged over the time interval τ are constant for a given σ_s:

$$I_R = \Delta h_c \frac{1}{\tau}\int_0^\tau \dot{m}''_s \mathrm{d}t = \frac{\Delta h_c(1-\chi_{char})w_s}{\tau} = \frac{\Delta h_c(1-\chi_{char})w_s\sigma_s}{75\,600}. \tag{5}$$

The reaction intensity and the commonly used fireline intensity, I, are also related:

$$I = I_R d = I_R R\,\tau = \Delta h_c(1-\chi_{char})w_s R, \tag{6}$$

where $\Delta h_c(1-\chi_{char})w_s$ is the heat per unit area released in the combustion process (neglecting heat from char oxidation). The fireline intensity has a number of practical uses since it has been related to observed flame heights and to fire management guidelines (e.g. Chandler *et al.* 1983). By integrating I along the fire perimeter the total heat release rate, HRR, for that portion of the perimeter can be found. Boundary conditions on large scale atmospheric models require values of HRR.

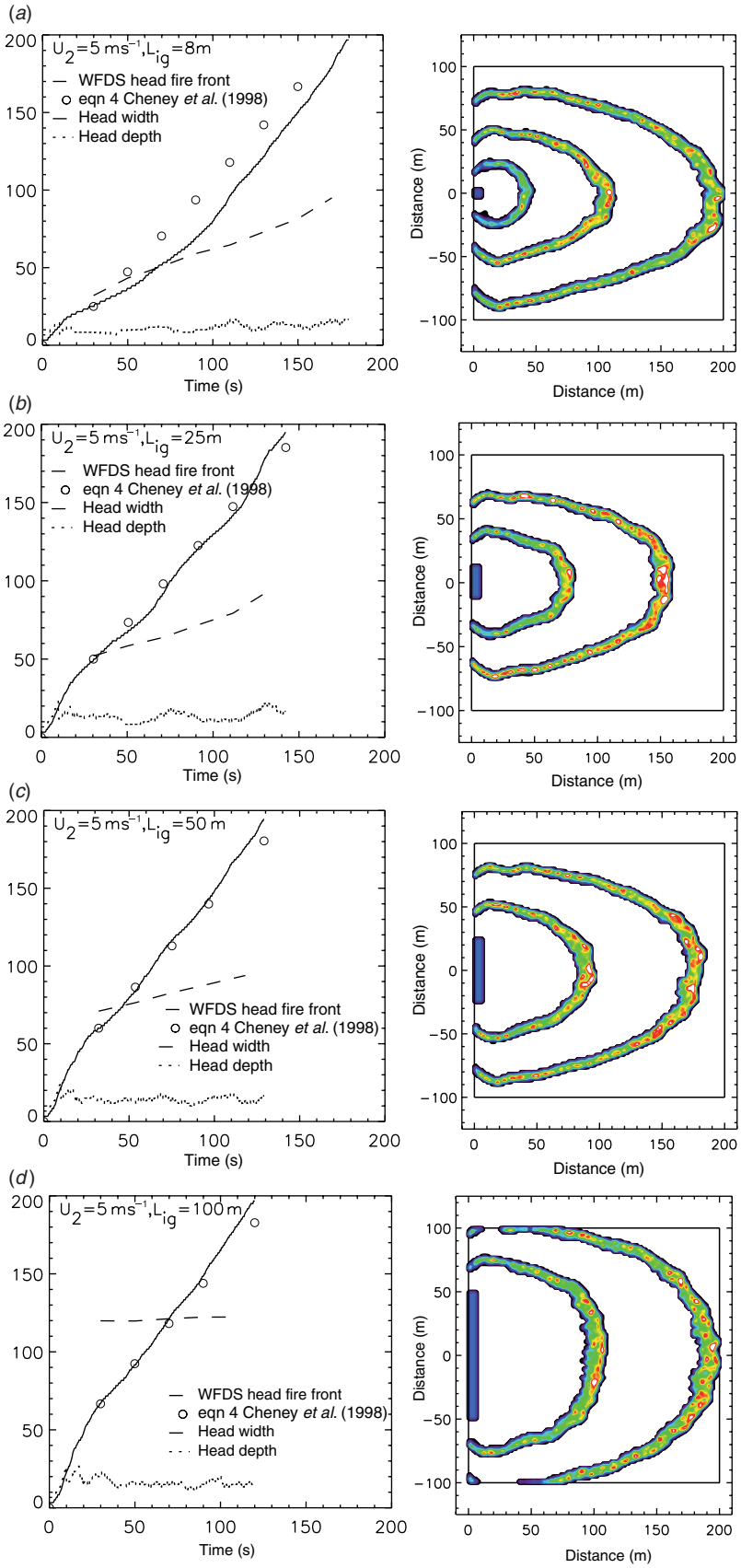

Fig. 9. Left column shows the location of the leading edge of the head fire versus time from WFDS (solid line) and from using Eqn (2) (circles), an empirical formula for the quasi-steady spread. The wind speed is $U_2 = 5\,\mathrm{m\,s^{-1}}$. Four ignition line fires L_{ig} are used: (*a*) 8 m, (*b*) 25 m, (*c*) 50 m, and (*d*) 100 m (same L_{ig} values as in Fig. 8). The width (dashed line) and depth (dotted line) of the head fire are also plotted. The fire perimeter (shaded contours of mass loss rate) for each case are shown in the right column at 60 s intervals, starting at 0 s. The fire spreads in a 200 × 200 m grassland plot with the fuel properties of experiment F19 listed in Table 1.

Fig. 11 shows the time history of WFDS predictions of $\dot{m}''_s$ spatially averaged over the fire beds of the head fire, the flanking fires, and entire fire perimeter. Two different wind cases U_2, each with $L_{ig} = 100$ m, are plotted. In each case, the average mass flux is largest in the head region of the fire perimeter, due to flame tilt. However, the flanking fires can be a greater portion of the entire fire line. This is the case for $U_2 = 5\ \mathrm{m\ s^{-1}}$, as seen in Fig. 9*d*. The total mass flux varies within 15% of its mean value for most of the $U_2 = 1\ \mathrm{m\ s^{-1}}$ case (after the fluctuations from ignition have died off) and for the latter half of the $U_2 = 5\ \mathrm{m\ s^{-1}}$ case.

The total HRR of the head fire, the flanking fires, and the entire fire bed for the same two cases is displayed in Fig. 12. These HRR values are computed by summing the mass fluxes over each region of the actively burning fireline:

$$\mathrm{HRR_{FR}} = \int_{\mathrm{FR}} I\,\mathrm{d}\ell \cong \sum_{\mathrm{FR}} \Delta h_c (1 - \chi_{\mathrm{char}}) \dot{m}''_s \Delta x \Delta y,$$

where FR denotes the head fire or flank fire region of the fire line, and Δx, Δy are the horizontal dimensions of the grid. After the fire line reaches the edges of the grassland plot at approximately $t = 180$ s in the $U_2 = 1\ \mathrm{m\ s^{-1}}$ case (see Fig. 8*d*), the flanking fires begin shortening and eventually disappear, no longer contributing to the HRR in Fig. 12*a*. As the flanking fires shorten, the head fire lengthens and its HRR increases until, at $t = 350$ s, it spans nearly the entire 200 m grass plot. In Fig. 12*b* the stronger ambient wind lengthens the flanking fires (see Fig. 9*d*) causing their HRR (and therefore the total HRR) to increase over the latter part of the simulation.

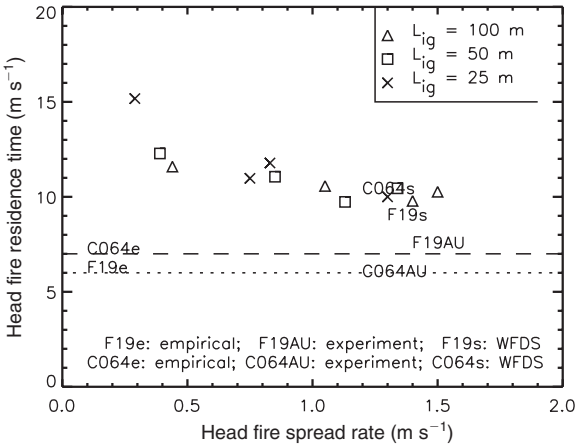

Fig. 10. Residence time, τ, from a number of sources. Symbols are $\tau = d/R$ where d and R are determined from WFDS simulations with $L_{ig} = 25$, 50, and 100 m during quasi-steady flame spread in a fuel bed with the characteristics of the F19 experiments. The dotted line (labelled 'F19e') and dashed line (labelled 'C064e') are residence times from the empirical formula Eqn (4) using σ_s from experiment F19 and C064 (see Table 1), respectively. F19s and C064s are $\tau = d/R$ values from WFDS simulations of experiments F19 and C064, respectively. F19AU and C064 are $\tau = d/R$ values from the experimentally measured d and R.

Case studies

The mechanism of fire spread can change along the fire perimeter depending on the wind speed. In zero ambient wind, entrainment by the fire creates a local wind into which the entire fire line spreads (backing fire). In the presence of an ambient wind, the downwind portion of the fire perimeter spreads with the wind (heading fire), the upwind portion of the fire perimeter spreads into the wind (backing fire), and the sides or flanks of the fire perimeter spread under conditions that can alternate between heading and backing fires. Note that in the cases considered here, there are no backing fires because ignition occurred along the fire

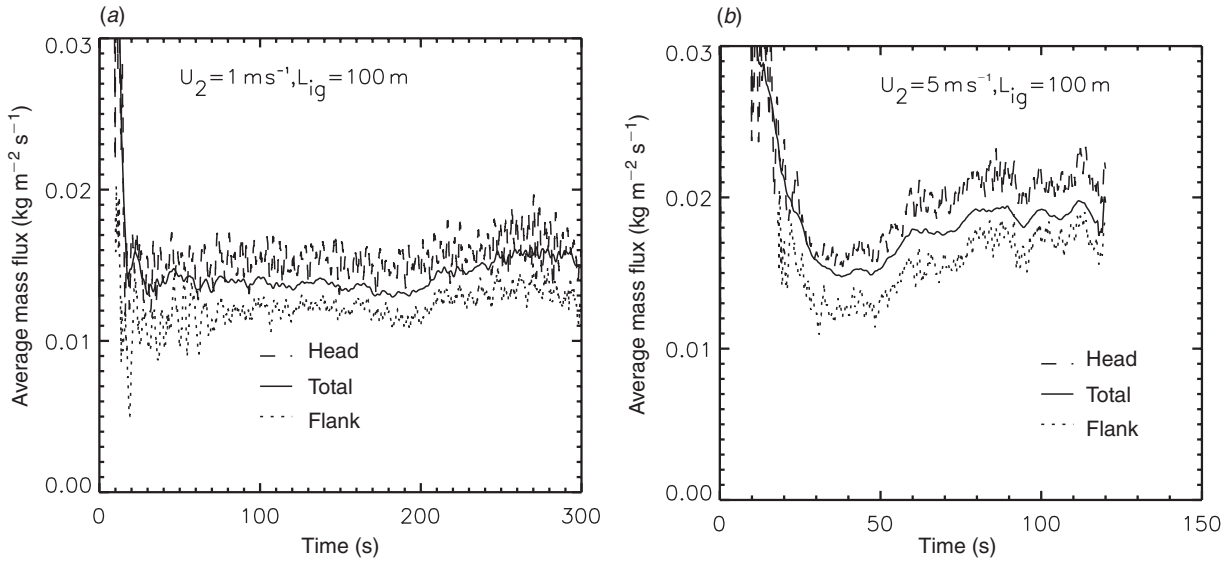

Fig. 11. WFDS time histories of the mass flux of fuel gases during pyrolysis, $\dot{m}''_{s,pyr}$, averaged over the head fire, flank fires, and the total fire perimeter. In both figures $L_{ig} = 100$ m. In both (*a*) and (*b*) the fuel bed has the characteristics of the grass in experiment F19 (Table 1). (*a*) $U_2 = 1\ \mathrm{m\ s^{-1}}$. (*b*) $U_2 = 5\ \mathrm{m\ s^{-1}}$.

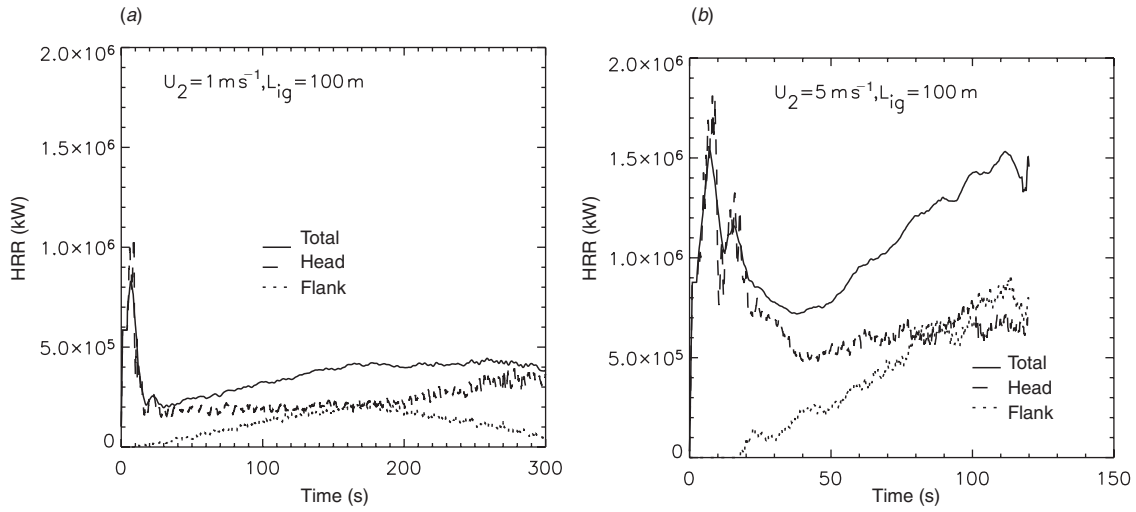

Fig. 12. WFDS time histories of the heat release rate, HRR, in the head fire, flank fires, and the total fire for the same cases shown in Fig. 11. In both, $L_{ig} = 100$ m. The fuel bed has the same characteristics as the grass in experiment F19 (Table 1). (*a*) $U_2 = 1\,\mathrm{m\,s^{-1}}$. (*b*) $U_2 = 5\,\mathrm{m\,s^{-1}}$.

break at the upwind border of the plot. Backing fires, in which the flame tends to tilt away from the unburned fuel, can consume the fuel from the base upward, resulting in more complete fuel consumption. Heading fires, in which the flame tilts toward the unburned fuel, can be associated with lower fuel consumption because the grass ignites at the top and burns downward, covering the unburned fuel beneath with a protective coating of ash. The spread mechanism in a flank fire can involve, depending on the fire–wind interaction, both the burning downward mechanism of head fires and the burning upward mechanism of backing fires. Thus, modelling the evolution of the entire fire line is a greater challenge, due to the different spread mechanisms, than modelling the behaviour of just the head fire.

WFDS cannot directly resolve the details in the grass fuel bed that differentiate a backing fire from a heading fire because the entire fuel bed is unresolved on the gas phase computational grid. For example, the height of the first grid cell in WFDS simulations of experiment F19 is 1.4 m while the height of the grass is 0.51 m. However, the fire–atmosphere interactions that occur over larger scales are much better resolved. It is hoped that this level of resolution of the fire physics will be sufficient to capture the dynamics of the entire fire perimeter. It is important that a three-dimensional model predict the behaviour of the entire fire perimeter. Otherwise, the overall heat release rate, fuel consumption, and smoke generation will be (to some degree) incorrectly predicted. The potential for this was seen, for example, in Fig. 12*b* where the gradual lengthening of the flank fire increased the total HRR of the fire while the HRR contribution from the head fire remained constant. These global fire characteristics are particularly important inputs to landscape and regional smoke transport models, which do not attempt to model the fire–fuel physics. In addition, the mechanisms behind extreme fire behaviour (such as blow-ups) are still poorly understood. A model that simulates the behaviour of the entire fire perimeter, as opposed to only the head fire, is more likely to shed light on these issues.

In this section, model predictions of fire perimeters from two experimental cases are presented. In the first experiment, called F19, the fuel is *Themeda* grass ($\sigma_s = 12\,240\,\mathrm{m^{-1}}$). The grassland plot is 200 × 200 m and the ignition line fire is 175 m long. This line fire was created with drip torches carried by two field workers walking for 56 s (88 m) in opposite directions from the center point to the ends of the line fire. The average wind speed, measured at the corners of the grassland plot and not including measurements influenced by the fire, equaled $4.8\,\mathrm{m\,s^{-1}}$. In the second experiment considered, called C064, the fuel is *Eriachne* grass ($\sigma_s = 9770$). This grass was cut to 50% of its height with the cuttings removed. The grassland plot is 104 × 108 m and the ignition line was 50 m long. The ignition line fire was created with drip torches carried by field workers walking in opposite directions for 26 s (25 m). The average wind speed was $4.6\,\mathrm{m\,s^{-1}}$. Fuel bed characteristics are given in Table 1 for both experiments. WFDS simulates the ignition procedure by sequentially igniting strips of the fuel bed at a rate that matches the experimental procedure. An animation of the WFDS fireline and smoke plume for case F19 can be found at Mell *et al*. (2007).

The time history of U_2 from WFDS and experiment F19 and C064 are shown in Figs 13*a* and 14*a*, respectively. The experimental value of U_2 (filled circles) is the average of the magnitude of the velocity vector, averaged over 5 s, in the horizontal plane $z = 2$ m measured every 5 s at the two upwind corners of the grassland plot. The WFDS value of U_2 is the magnitude of the simulated velocity vector at the y midpoint of the ignition line fire and at a height of $z = 2.1$ m and $z = 1.95$ m for cases F19 and C064, respectively.

WFDS velocity vector components in the horizontal plane $z \cong 2$ m are shown in Figs 13*b* and 14*b* for cases F19 and C064, respectively. Also shown is the outer boundary of the flaming region in the same plane, $z \cong 2$ m. Case F19 clearly has a larger fire perimeter. The F19 fireline also presents a greater blockage to the ambient wind as can be seen by the smaller vector lengths in Fig. 13*b*, compared to Fig. 14*b*, upwind of the head

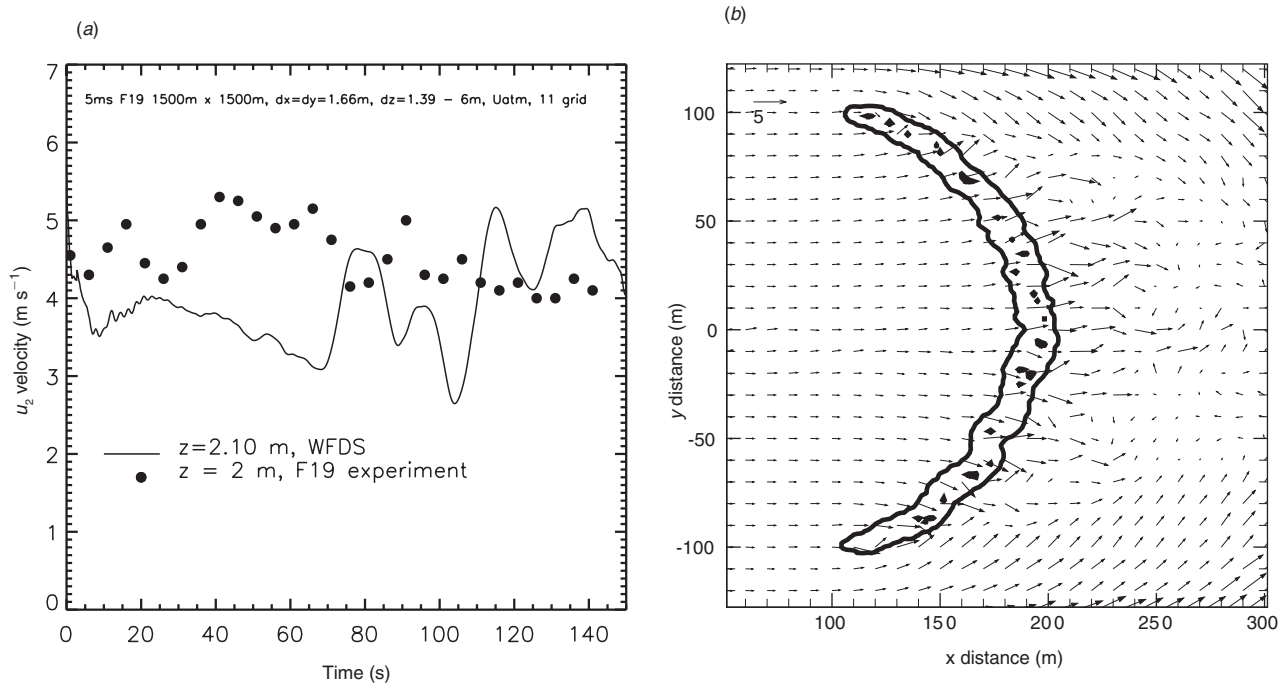

Fig. 13. WFDS and experimental results for experiment F19 at $t = 100$ s. The ignition line fire was located at $50\text{ m} \le x \le 53.3\text{ m}$, $-86.7\text{ m} \le y \le 86.7\text{ m}$. (*a*) Time history of U_2. WFDS predictions averaged over 5 s (solid line) are located at a height of $z = 2.1$ m above the midpoint of the ignition line (point $x = 50$, $y = 0$ in [*b*]). Field measurements (filled circles) are the average of measurements taken every 5 s at $z = 2$ m at the upwind corners of the 200 m × 200 m grassland plot ($x = 50$ m, $y = -100$ m, 100 m in [*b*]). (*b*) Velocity vectors at a height of 2.1 m from WFDS at time $t = 100$ s. Contour of the heat release rate showing borders of the flaming region in the same plane is also shown. The WFDS grassland plot is located at $50\text{ m} \le x \le 250\text{ m}$, $-100\text{ m} \le y \le 100\text{ m}$.

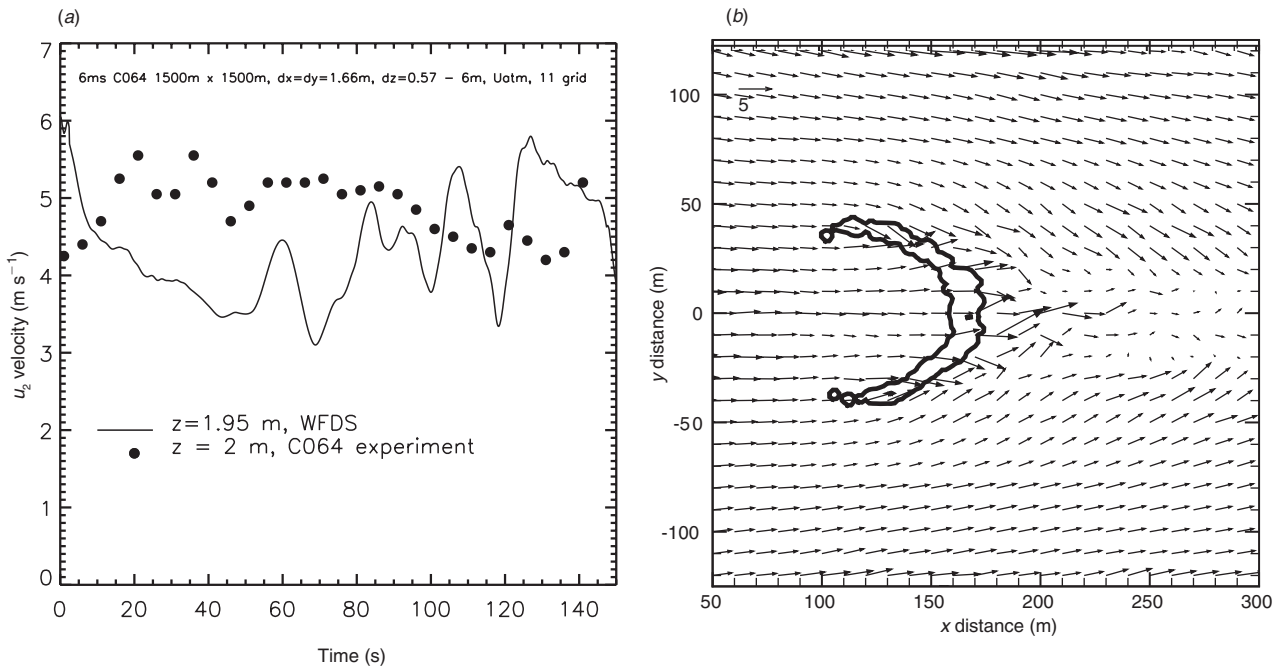

Fig. 14. WFDS and experimental results for experiment C064 at $t = 75$ s. The ignition line fire was located at $100\text{ m} \le x \le 101.6\text{ m}$, $-25\text{ m} \le y \le 25\text{ m}$. (*a*) Time history of U_2. WFDS predictions averaged over 5 s (solid line) are located at a height of $z = 1.95$ m above the midpoint of the ignition line (point $x = 100$, $y = 0$ in [*b*]). Field measurements (filled circles) are the average of measurements taken every 5 s at $z = 1.95$ m at the upwind corners of the 104 × 108 m grassland plot ($x = 100$ m, $y = -52$ m, 52 m in [*b*]). (*b*) Velocity vectors at a height of 2.0 m from WFDS at time $t = 100$ s. Contour of the heat release rate showing borders of the flaming region in the same plane is also shown. The WFDS grassland plot is located at $100\text{ m} \le x \le 202\text{ m}$, $-53\text{ m} \le y \le 53\text{ m}$.

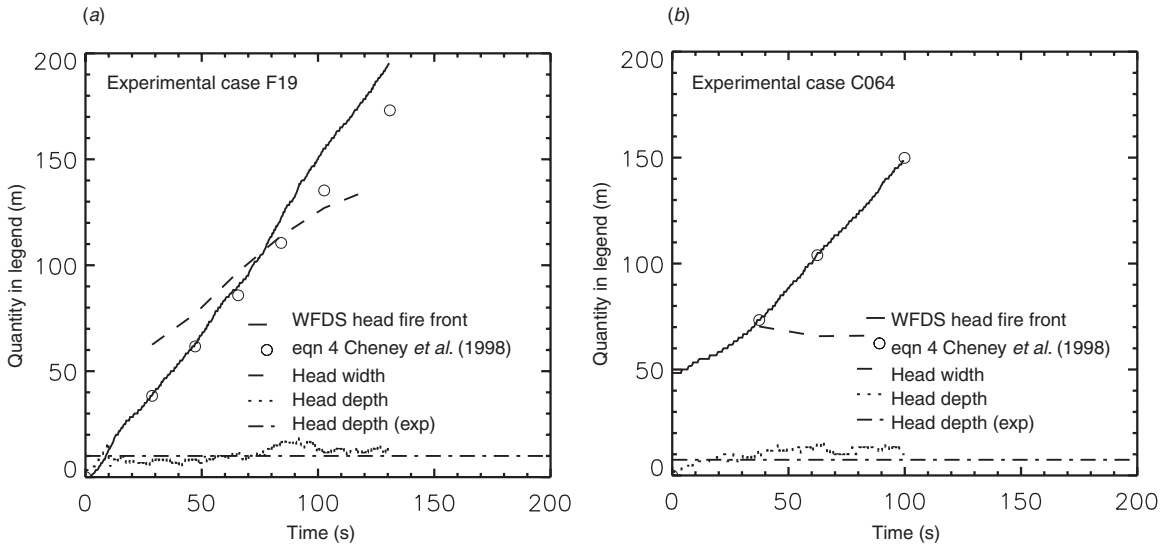

Fig. 15. Time histories of the location of the leading edge, the width, and the depth of the head fire for experiments (*a*) F19 and (*b*) C064. The leading edge of the head fire from WFDS is shown as a solid line and as filled circles using the empirical spread rate formula, Eqn (2), with WFDS values for the head width, *W*. The head width from WFDS is a dashed line and the instantaneous depth a dotted line. The average head fire depth from field measurements is a dash-dot line.

fire. Entrainment of air toward the fire from the far-field can be clearly seen.

The location of the leading edge of the head fire versus time, from both WFDS (solid line) and by using Eqn (2) (circles) for both experimental cases F19 and C064 is shown in Fig. 15*a*, *b*, respectively. The head width from WFDS is plotted as a dashed line. The head depth from both WFDS (dotted line) and its average value from the experiments (dash-dot line) are also shown. The average value of the WFDS head fire depths is 11.4 m for case F19 (experimental value was 10 m) and 12.2 m for case C064 (experimental value was 7.1 m). Overall, the spread rate of both cases agrees well with the empirical formula, Eqn (2). During the period of transient behaviour in case F19, $76\text{ s} \leq t \leq 90\text{ s}$ in Fig. 15*a*, the simulated flanking fires reach the boundaries of the grassland plot and extinguish. Before and after this period the simulated flame spread rate is nearly constant and in good agreement with Eqn (2).

The fire perimeters of cases F19 and C064 are shown in Fig. 16*a*, *b*, respectively. The actively burning fire bed from WFDS is shown as shaded contours. The leading edge of the head fire from the experiments is plotted as symbols. In F19 a wind shift occurs in the experiment after $t = 86$ s, which breaks the symmetry of the fire perimeter. This does not occur in WFDS since a constant wind orientation is assumed at the inflow boundary. As expected from the previous results, the spread of the head fire is well predicted at all times. The simulated fire reaches the downwind fire break at 133 s; the experimental fire at 138 s. Before the wind shift, the predicted fire perimeter closely matches the measured fire perimeter. After $t = 86$ s it is not clear how well WFDS predicts the entire fireline because the wind shift significantly changes the observed fire perimeter. Also, long flanking fires (as, for example, those shown in Fig. 9*c*) do not develop for this case because the flank fires reach the fire breaks relatively soon.

In case C064, shown in Fig. 16*b*, extended free burning flank fires do develop. The spread rate of the head fire is well predicted. WFDS overpredicts the spread rate of the flank fires. The reasons for this are the subject of ongoing model development efforts. The current version of WFDS does not faithfully model the upward spread mechanism that can be present in flank fires. Instead, the fire burns downward through the grassland fuel bed everywhere along the perimeter. Also, flank fire depths in the field were observed to be significantly smaller than head fire depths. The horizontal grid resolutions used here (1.66 m) adequately resolve the head fire depth but this may not be the case for the flank fires.

Plots of the spatially averaged mass flux in the head and flank fire regions of the fire perimeter and the total perimeter for case F19 and C064 are presented in Fig. 17*a*, *b*, respectively. Case C064 has a smaller mass flux, which is consistent with its smaller fuel load. The initial period of larger mass flux in F19 ($t < 60$ s) is due to the ignition line fire. The ignition procedure stops at $t = 56$ s. Fig. 18 shows the heat release rates associated with the entire fire perimeter and the head and flanking fires for both experimental cases. The HRR in case C064 is significantly smaller than F19 due to its lighter fuel loading and shorter fireline perimeter. In case F19, the flanking fires dominate the total HRR during the ignition phase. During the latter part of the F19 case HRR $\cong 1.4$ GW (or $I_R = 350\text{ kW m}^{-2}$). For comparison, estimates of I_R during the burning of logging slash are approximately $I_R = 75\text{ kW m}^{-2}$ (Ohlemiller and Corley 1994). The actively burning area in the logging slash fire was $\sim 2 \times 10^5\text{ m}^2$. This is 50 times larger than the actively burning area in the latter half of the F19 simulation. For this reason the total HRR in the logging slash fires was 15 GW, approximately ten times larger than the F19 grassland fire.

The spatially averaged head fire mass flux in Fig. 17 is used in Eqn (5) to determine the time history of I_R for the head

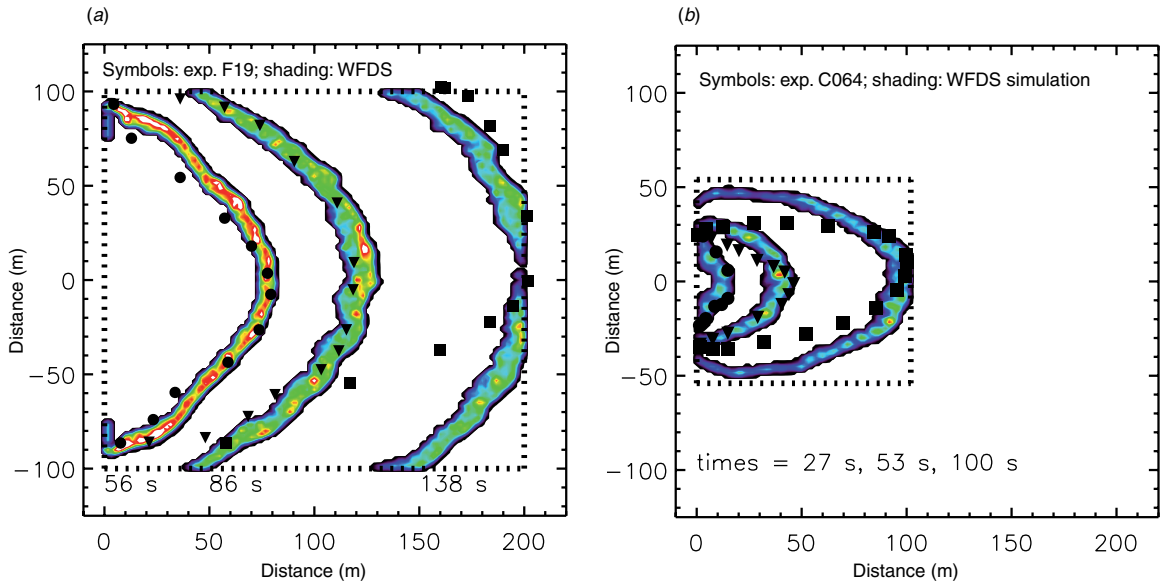

Fig. 16. Shaded contours show the actively burning fire bed (non-zero mass flux of gaseous fuel) from WFDS; symbols show the leading edge of the observed fire front for experiments (*a*) F19 and (*b*) C064. The borders of the grassland plot are represented by the dashed line. See text for details and Table 1 for fuel/environmental parameters.

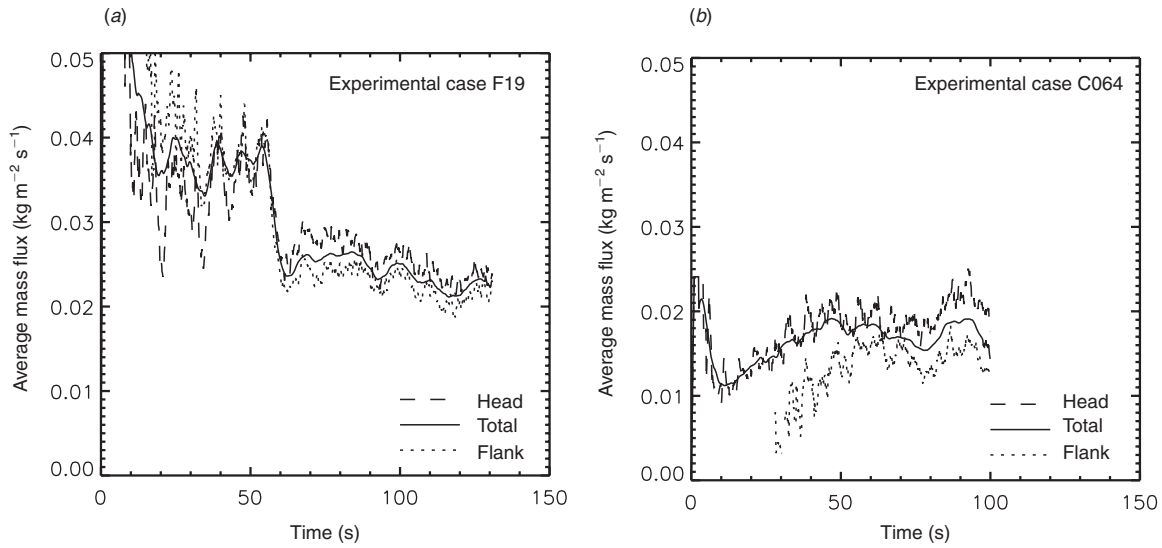

Fig. 17. WFDS time histories, for experimental cases F19 and C064, of the mass flux of fuel gases during pyrolysis, $\dot{m}''_{s,pyr}$ (kg m^{-2} s^{-1}), averaged over the head fire, flank fires, and the total fire perimeter. In both figures, $L_{ig} = 100$ m. (*a*) Experimental case F19. (*b*) Experimental case C064.

fire (not shown). The time history of I for the head fire is then determined from I_R and d by using Eqn (6). The resulting head-fireline intensity is plotted (solid line) in Fig. 19 for cases F19 and C064, respectively. Also plotted are the values of I determined from the experimentally observed head fire spread rates using the last relation on the right-hand-side of Eqn (6) (line labelled 'R based') and from the semi-empirical model BehavePlus (line labelled 'BEHAVE'). The experimentally observed head fire spread rates are $R = 1.4$ and $1.2\,\mathrm{m\,s^{-1}}$, for F19 and C064, respectively. For these experimental conditions the simple approach using the head fire spread rate provided a better estimate of I than BehavePlus. The BehavePlus values were obtained by using the experimentally measured values of fuel load, moisture, surface-to-volume ratio, and fuel bed depth that are listed in Table 1, and the average of measured values for the moisture of extinction (22%; Cheney *et al.* 1998). The mid-flame wind speeds of $4.4\,\mathrm{m\,s^{-1}}$ for F19 and $2.8\,\mathrm{m\,s^{-1}}$ for C064 were used. The dead fuel heat content was $18\,608\,\mathrm{kJ\,kg^{-1}}$, which

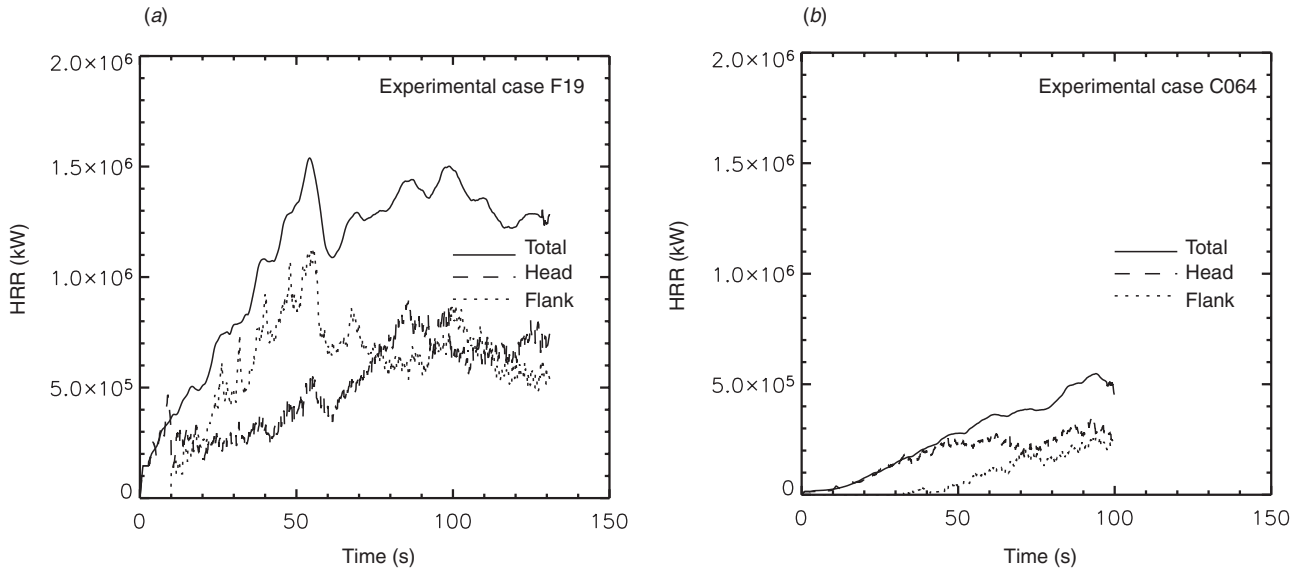

Fig. 18. WFDS time histories, for experimental cases F19 and C064, of the heat release rate, HRR, in the head fire, flank fires, and the total fire. (*a*) Experimental case F19. (*b*) Experimental case C064.

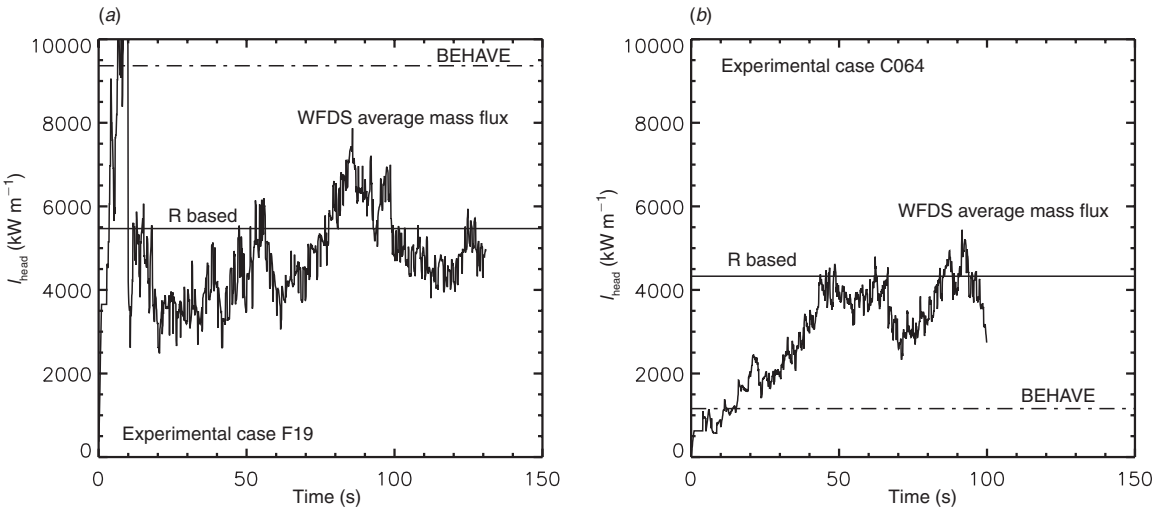

Fig. 19. Time history, for experimental cases F19 and C064, of the fire line intensity, I, in the head fire region of the fire perimeter. Solid line is from WFDS. The value of I from BehavePlus (line labelled 'BEHAVE') and from $I = \Delta h_c(1 - \chi_{char})w_s R$ using the experimentally measured R (line labelled 'R based'; Eqn 6) are also shown. (*a*) Experimental case F19. (*b*) Experimental case C064.

is listed in NFFL descriptions for grass fuels (UCSB 2005). BehavePlus predictions of the head-fireline intensity are nearly a factor of two too large for case F19 and a factor of four too small for case C064. This is due to BehavePlus overpredicting the spread rate for F19 ($R = 4.4\,\mathrm{m\,s^{-1}}$) and underpredicting it for C064 ($R = 0.47\,\mathrm{m\,s^{-1}}$). This is relevant to mesoscale coupled atmosphere–fire models currently under development (e.g. Clark *et al.* 2003, 2004; Coen 2005) as their heat and mass fluxes from the fire into the atmosphere are based in part on spread rate predictions from empirical and semi-empirical spread rate formulas. These results imply that, for Australian grassland fuels, the empirical fire spread formula should be used rather than the semi-empirical (Rothermel 1972) spread rate.

Summary and conclusions

A physics-based, transient, three-dimensional, coupled fire–atmosphere model for simulating fire spread through surface fuels on flat terrain was developed and evaluated using observational data from Australian grassland fires. This model, called WFDS, is an extension, to vegetative fuels, of the structural FDS developed at NIST. Grassland fires were chosen here because of

the simplicity of both the fuel and terrain, and because a significant amount of experimental data (for Australian grassland fires) exists for model validation.

Sixteen fires (four different ignition line lengths and four different wind speeds) were simulated. Head fire spread rates from WFDS were compared to an empirical relation developed from experimental data. Overall, WFDS predictions of the dependence of the head fire spread rate on both the ambient wind speed and on the head fire width were similar to an empirical relation.

Two specific Australian grassland experiments were also simulated. In both cases the location of the head fire was well predicted. One experimental case had extended, freely spreading, flank fires. WFDS overpredicted the spread rate of these flank fires. The reasons for this are under investigation. One possibility is that flank fires are under resolved, since their fire depth can be significantly smaller than head fires. Some light may be shed on this issue by comparing to a larger number of experimental fires. We plan to extend the validation effort to a larger set of experiments and to a wider range of fuel parameters (moisture, surface to volume ratio, packing ratio) in order to better assess WFDS capabilities.

Areas for further model development and model evaluation include:

- The vegetation model is not appropriate for fuels through which significant vertical flame spread can occur. A model approach for suspended vegetation, such as tree crowns, has been implemented and is currently being evaluated. Preliminary results can found in Mell *et al.* (2007).
- The grassland fuel bed is assumed to burn from the top down. This is consistent with field observations of head fires, which spread with the ambient wind. It is not consistent with backing or flanking fire behaviour, based on observations. This may play a role in the overprediction of flank fire spread rates.
- Char oxidation has not been considered. For this reason, smouldering or glowing combustion of the fuel after the fire front has passed is not present. This can be an important contribution to overall smoke generation.
- The underestimation of convective heat transfer into the solid fuel in regions of active combustion, and the sensitivity of the results to changes in how the drag and convective heat transfer is modelled needs further investigation.
- A more complete evaluation of the model's performance for a range of fuel and environmental parameters (e.g. moisture level, surface-to-volume ratios, bulk fuel loadings, wind speeds, and wind profiles) is required.

Multidimensional numerical fluid-dynamical wildfire simulation models can be used to study the behaviour of wildfire and wildland–urban interface fires. However, depending on the scope of the physical models employed they can require computational resources that preclude real-time forecasts. Such is the case with the version of WFDS presented here. This model, therefore, has not been designed to replace operational models, but it can be used to expand or improve their capabilities.

The computational cost of physics-based wildland fire modelling limits the application of the approach to modelling wildfire behaviour within a certain scale range. In models like WFDS, computational resources are devoted to resolving fire combustion and the close-in fire–atmosphere flow. In large-scale coupled atmosphere–wildfire models the thermal degradation of solid fuel is not modelled directly and combustion is parameterised. Empirical or semi-empirical models for fire spread rates and heat and mass fluxes from the fire to the atmosphere are used (Clark *et al.* 1996, 2003, 2004; Coen 2005). Computational resources can then be devoted to resolving the large scale fire–atmospheric physics.

Large scale fire–atmosphere interactions are considered to be of major importance to predicting fire behaviour, especially severe fire behaviour. A longer-term goal, therefore, is to develop and test (using WFDS) improved models of fire physics suitable for use in large scale atmosphere–wildfire models. Once suitably validated, both the WFDS and a large-scale coupled atmosphere–wildfire model can be used to evaluate operational models over a wide range of conditions and real-time applications, such as prediction of firebrand generation and transport, and fire spread rates. They can also be used to improve our understanding of how fuel conditions (amount, type, moisture content), terrain and weather are responsible for severe and blow-up fires.

Another long-term goal at NIST is the development of a simulation tool for wildland–urban interface fires. The cost in insured damages from these fires can significantly outweigh the operational costs of fighting the fire. The fuels in these fires are an intermix of continuous and discrete vegetative fuels and structural materials. These fuel types, and their spatial arrangement, fall outside traditional wildland fuel classification methods and, therefore, current fire-risk assessment methods or models. A suitably validated simulation tool could be used to help determine and assess the important risk factors in existing and planned communities.

Accessory Publication

An Accessory Publication, which covers the approaches for modelling the gas phase and the solid fuel, is available from the *International Journal of Wildland Fire* website.

Acknowledgements

The first author would like to thank Dr Ron Rehm of NIST for many fruitful discussions during the writing of this paper. This work was sponsored in part by the USDA Forest Service Joint Venture Agreement 03-JV-11231300-088.

References

Albini FA (1976) Estimating wildfire behavior and effects. USDA Forest Service, Intermountain Forest and Range Experiment Station General Technical Report INT-30. (Ogden, UT)

Albini FA (1985) A model for fire spread in wildland fuels by radiation. *Combustion Science and Technology* **42**, 229–258.

Albini FA (1993) Dynamics and modeling of vegetation fires: observations. In 'Fire in the Environment: The Ecological, Atmospheric, and Climatic Importance of Vegetation Fires'. (Eds PJ Crutzen, JG Goldammer) pp. 39–52. (John Wiley and Sons: Chichester)

Anderson HE (1969) Heat transfer and fire spread. USDA Forest Service, Intermountain Forest and Range Experiment Station General Technical Report INT-69. (Ogden, UT)

Andrews PL (1986) BEHAVE: Fire behavior prediction and modeling system – BURN subsystem part 1. USDA Forest Service, Intermountain Forest and Range Experiment Station General Technical Report INT-194. (Ogden, UT)

Andrews PL, Bevins CD, Seli RC (2003) BehavePlus fire modeling system, version 2.0: User's Guide. USDA Forest Service, Rocky Mountain Research Station General Technical Report RMRS-GTR-106WWW. (Ogden, UT)

Bankston CP, Zinn BT, Browner RF, Powell EA (1981) Aspects of the mechanisms of smoke generation by burning materials. *Combustion and Flame* **41**, 273–292. doi:10.1016/0010-2180(81)90062-6

Beer T (1991) The interaction of wind and fire. *Boundary-Layer Meteorology* **54**, 287–308. doi:10.1007/BF00183958

Chandler C, Cheney P, Thomas L, Trabaud P, Williams D (1983) Chemistry and physics of ignition and combustion. In 'Fire in Forestry'. pp. 1–30. (John Wiley & Sons: New York)

Cheney NP, Gould JS (1995) Fire growth in grassland fuels. *International Journal of Wildland Fire* **5**, 237–247. doi:10.1071/WF9950237

Cheney NP, Gould JS, Catchpole WR (1993) The influence of fuel, weather and fire shape variables on fire spread in grasslands. *International Journal of Wildland Fire* **3**, 31–44. doi:10.1071/WF9930031

Cheney NP, Gould JS, Catchpole WR (1998) Prediction of fire spread in grasslands. *International Journal of Wildland Fire* **8**, 1–13. doi:10.1071/WF9980001

Clark TL, Jenkins MA, Coen J, Packham D (1996) A coupled atmospheric-fire model: Convective feedback on fire-line dynamics. *Journal of Applied Meteorology* **35**, 875–901. doi:10.1175/1520-0450(1996)035<0875:ACAMCF>2.0.CO;2

Clark TL, Griffths M, Reeder MJ, Latham D (2003) Numerical simulations of grassland fire in the Northern Territory, Australia: A new subgrid-scale fire parameterization. *Journal of Geophysical Research* **108**, 4589. doi:10.1029/2002JD003340

Clark TL, Coen JL, Latham D (2004) Description of a coupled atmosphere-fire model. *International Journal of Wildland Fire* **13**, 49–63. doi:10.1071/WF03043

Coen J (2003) Simulation of wildfire incidents using coupled atmosphere–fire modeling. In 'Second International Wildland Fire Ecology and Fire Management Congress and Fifth Symposium of Fire on Forest Meteorology'. Paper J2.4. (American Meteorological Society) Available at http://ams.confex.com/ams/pdfpapers/65709.pdf [Verified 18 October 2006]

Coen J (2005) Simulation of the Big Elk Fire using coupled atmosphere-fire modeling. *International Journal of Wildland Fire* **14**, 49–59. doi:10.1071/WF04047

Colman JJ, Linn RR (2003) Non-local chemistry implementation in HIGRAD/FIRETEC. In '5th Symposium on Fire and Forest Meteorology'. Available at http://ams.confex.com/ams/FIRE2003/techprogram/paper_65955.htm [Verified 18 October 2006]

Colman JJ, Linn RR (2005) Separating combustion from pyrolysis in HIGRAD/FIRETEC. In '6th Symposium on Fire and Forest Meteorology'. Available at http://ams.confex.com/ams/6FireJoint/techprogram/paper_97650.htm [Verified 18 October 2006]

Costa AM, Pereira JCF, Siqueira M (1995) Numerical prediction of fire spread over vegetation in arbitrary 3D terrain. *Fire and Materials* **19**, 265–273. doi:10.1002/FAM.810190605

Davis KP (1959) 'Forest Fire: Control and Use.' (McGraw-Hill: New York)

De Mestre NJ, Catchpole EA, Anderson DH, Rothermel RC (1989) Uniform propagation of a planar fire front without wind. *Combustion Science and Technology* **65**, 231–244.

Dupuy JL, Morvan D (2005) Numerical study of the a crown fire spreading toward a fuel break using a multiphase physical model. *International Journal of Wildland Fire* **14**, 141–151. doi:10.1071/WF04028

Finney MA (1998) FARSITE: Fire area simulator-model, development and evaluation. USDA Forest Service, Rocky Mountain Research Station Research Paper RMRS-RP-4. (Ogden, UT)

Fons WL (1946) Analysis of fire spread in light forest fuels. *Journal of Agricultural Research* **72**, 93–121.

Forney GP, McGrattan KB (2004) User's guide for smokeview version 4: A tool for visualizing fire dynamics simulation data. Technical Report NISTIR, Special Publication 1017. (National Institute of Standards and Technology: Gaithersburg, MD) Available at http://www.fire.nist.gov/fds/docs/sv_users_guide_4.pdf [Verified 18 December 2006]

GAO (1999) Western national forests: A cohesive strategy is needed to address catastrophic wildfire threats. Technical Report GAO/RCED-99-65. (United States General Accounting Office: Washington, DC)

GAO (2005) Technology assessment: protecting structures and improving communications during wild-land fires. Technical Report GAO-05-380. (United States Government Accountability Office: Washington, DC)

Gould JS (1988) Validation of the Rothermel fire spread model and related fuel parameters in grasslands fuels. In 'Proceedings of the Conference on Bushfire Modelling and Fire Danger Rating Systems', 11–12 July 1988. (CSIRO: Canberra)

Grishin AM (1996) Mathematical modelling of forest fires. In 'Fire in Ecosystems of Boreal Eurasia'. (Ed. V Furyaev) pp. 314–325. (Kluwer Academic Publishers: Dordrecht, the Netherlands)

Grishin AM, Gruzin AD, Zverev VD (1985) Study of the structure and limits of propagation of the front of an upstream forest fire. *Combustion, Explosion, and Shock Waves* **21**, 9–18.

Hirsch KG (1996) Canadian forest fire behavior prediction (FBP) system: user's guide. Special Report 7. Canadian Forest Service, Northwest Region, Northern Forestry Centre. (Edmonton, AB)

Hough WQ (1969) Caloric value of some forest fuels of the southern United States. USDA Forest Service, Southeastern Forest Experiment Station Research Note SE-120. (Asheville, NC) Available at http://www.srs.fs.usda.gov/pubs/2778 [Verified 18 October 2006]

Incropera FP, Dewitt DP (1996) 'Fundamentals of Heat and Mass Transfer.' (John Wiley & Sons: New York)

Johnson EA, Miayanishi K (Eds) (2001) 'Forest Fires: Behavior and Ecological Effects.' (Academic Press: San Diego)

Larini M, Giroud F, Porterie B, Loraud J-C (1998) A multiphase formulation for fire propagation in heterogeneous combustible media. *International Journal of Heat and Mass Transfer* **41**, 881–897. doi:10.1016/S0017-9310(97)00173-7

Linn RR (1997) A transport model for prediction of wildfire behavior. PhD thesis, New Mexico State University.

Linn R, Cunningham P (2005) Numerical simulations of grass fires using a coupled atmosphere–fire model: Basic fire behavior and dependence on wind speed. *Journal of Geophysical Research* **110**, D13107. doi:10.1029/2004JD005597

Linn R, Reisner J, Colman JJ, Winterkamp J (2002) Studying wildfire behavior using FIRETEC. *International Journal of Wildland Fire* **11**, 233–246. doi:10.1071/WF02007

Margerit J, Sero-Guillaume O (2002) Modelling forest fires: Part II: reduction to two-dimensional models and simulation of propagation. *International Journal of Heat and Mass Transfer* **45**, 1723–1737. doi:10.1016/S0017-9310(01)00249-6

McGrattan KB (Ed.) (2004) Fire Dynamics Simulator Version 4: Technical Reference Guide. NISTIR, Special Publication 1018. (National Institute of Standards and Technology: Gaithersburg, MD) Available at http://www.fire.nist.gov/fds/docs/fds_tech_guide_4.pdf [Verified 18 December 2006]

Mell WE, McGrattan KG, Baum HR (1996) Numerical simulation of combustion in fire plumes. *Proceedings of the Combustion Institute* **26**, 1523–1530.

Mell WE, Charney JJ, Jenkins MA, Cheney P, Gould J (2005) 'Numerical simulations of grassland fire behavior from the LANL-FIRETEC and NIST-WFDS models.' EastFIRE Conference, 11–13 May, George Mason University, Fairfax, VA.

Mell W, Maranghides A, Rehm R, Manzello S, Forney G, Jenkins MA, Sun R, Krueger S (2007) 'Wildland–Urban Interface and Wildland

Fires.' Available at http://www2.bfrl.nist.gov/userpages/wmell/public.html [Verified January 2007]

Morvan D, Dupuy JL (2001) Modeling fire spread through a forest fuel bed using a multiphase formulation. *Combustion and Flame* **127**, 1981–1984. doi:10.1016/S0010-2180(01)00302-9

Morvan D, Dupuy JL (2004) Modeling the propagation of a wildfire through a Mediterrean shrub using a multiphase formulation. *Combustion and Flame* **138**, 199–210. doi:10.1016/J.COMBUSTFLAME.2004.05.001

Morvan D, Tauleigne V, Dupuy JL (2002*a*) 'Flame Geometry and Surface to Crown Fire Transition During the Propagation of a Line Fire Through a Mediterranean Shrub.' (Millpress: Rotterdam)

Morvan D, Tauleigne V, Dupuy JL (2002*b*) 'Wind Effects on Wildfire Propagation Through a Mediterranean Shrub.' (Millpress: Rotterdam)

Murphy PJ, Mudds JP, Stocks BJ, Kasischke ES, Barry D, Alexander ME, French NHF (2000) Historical fire records in the North American boreal forest. In 'Ecological Studies, Vol. 138, Fire, Climate Change, and Carbon Cycling in the Boreal Forest'. (Eds ES Kasischke, BJ Stocks) pp. 274–288. (Springer-Verlag: New York)

Noble IR, Bary GAV, Gill AM (1980) McArthur's fire-danger meters expressed as equations. *Australian Journal of Ecology* **5**, 201–203. doi:10.1111/J.1442-9993.1980.TB01243.X

Ohlemiller T, Corley D (1994) Heat release rate and induced wind field in a large scale fire. *Combustion Science and Technology* **97**, 315–330.

Pagni PJ, Peterson TG (1973) Fire spread through pourous fuels. *Proceedings of the Combustion Institute* **14**, 1099–1107.

Parker WJ (1989) Prediction of the heat release rate of douglas fir. In 'Fire Safety Science – Proceedings of the 2nd International Symposium', Tokyo, 13–17 June 1998. (Eds T Wakamatsu, Y Hasemi, A Sekizawa, PG Seeger, PJ Pagni, CE Grant) pp. 337–346. (Hemisphere Publishing: New York)

Pastor E, Zarate L, Planas E, Arnaldos J (2003) Mathematical models and calculations systems for the study of wildland fire behavior. *Progress in Energy and Combustion Science* **29**, 139–153. doi:10.1016/S0360-1285(03)00017-0

Pitts WM (1991) Wind effects on fires. *Progress in Energy and Combustion Science* **17**, 83–134. doi:10.1016/0360-1285(91)90017-H

Porterie B, Morvan D, Larini M, Loraud JC (1998) Wildfire propagation: a two-dimensional multiphase approach. *Combustion, Explosion and Shock Waves* **34**, 139–150.

Porterie B, Morvan D, Loraud JC, Larini M (2000) Firespread through fuel beds: Modeling of wind-aided fires and induced hydrodynamics. *Physics of Fluids* **12**, 1762–1782.

Quintiere JG (1997) 'Principles of Fire Behavior.' (Delmar Publishers: Albany)

Reisner J, Wynne S, Margolin L, Linn R (2000) Coupled atmosphere-fire modeling employing the method of averages. *Monthly Weather Review* **128**, 3683–3691. doi:10.1175/1520-0493 (2001)129<3683:CAFMET>2.0.CO;2

Rothermel RC (1972) A mathematical model for predicting fire spread in wildland fuels. USDA Forest Service, Intermountain Forest and Range Experiment Station General Technical Report INT-11. (Ogden, UT)

Sero-Guillaume O, Margerit J (2002) Modelling forest fires: Part I: a complete set of equations derived by extended irreversible thermodynamics. *International Journal of Heat and Mass Transfer* **45**, 1705–1722. doi:10.1016/S0017-9310(01)00248-4

Sneeuwjagt RJ, Frandsen WH (1977) Behavior of experimental grass fires vs. predictions based on Rothermel's fire model. *Canadian Journal of Forest Research* **7**, 357–367.

Stephens GL (1984) The parameterization of radiation for numerical weather prediction and climate models. *Monthly Weather Review* **112**, 826–867. doi:10.1175/1520-0493(1984)112<0826:TPORFN>2.0.CO;2

Stewart S, Radeloff V, Hammer R (2003) Characteristics and location of the wildland–urban interface in the United States. In '2nd International Wildland Fire Ecology and Fire Management Congress', Orlando, FL, 19 November 2003. Available http://ams.confex.com/ams/pdfpapers/65316.pdf [Verified 18 December 2006]

Stock BJ, Simard AJ (1993) Forest fire management in Canada. *Disaster Management* **5**, 21–27.

Susott RA (1982) Characterization of the thermal properties of forest fuels by combustible gas analysis. *Forest Science* **2**, 404–420.

UCSB (2005) 'Southern California Wildfire Hazard Center.' (University of Southern California: Santa Barbara) Available at http://www.icess.ucsb.edu/resac/ [Verified 18 October 2006]

USDA Forest Service (2006) 'Policy Implications of Large Fire Management.' Available at http://www.fs.fed.us/fire/management/Large_Fire_Mgt.pdf [Verified 19 October 2006]

USFS BlueSky (2004) 'Bluesky Modeling Framework to Predict Cumulative Impacts of Smoke From Agricultural, Forest, and Range Fires.' Available at http://www.airfire.org/bluesky/ [Verified 18 October 2006]

Weber RO (1991) Modelling fire spread through fuel beds. *Progress in Energy and Combustion Science* **17**, 67–82. doi:10.1016/0360-1285(91)90003-6

Westerling AL, Hidalgo HG, Cayan DR, Swetnam TW (2006) Warming and earlier spring increases western US forest wildfire activity. *Science* **313**, 940–943.

Williams FA (1982) Urban and wildfire fire phenomenology. *Progress in Energy and Combustion Science* **8**, 317–354. doi:10.1016/0360-1285(82)90004-1

Zhou XY, Pereira JCF (2000) A multidimensional model for simulating vegetation fire spread using a porous media sub-model. *Fire and Materials* **24**, 37–43. doi:10.1002/(SICI)1099-1018(200001/02)24:1<37::AID-FAM718>3.0.CO;2-Q

Zicherman J (2004) Fire at the urban wildland interface: Performance of California homes and buildings. California Department of Forestry and Fire Protection, Technical Report IFB no. 5CA334189, FCA no. 05-6369. (Fire Cause Analysis: Richmond, CA)

Appendix 1

Nomenclature used in this paper.

$c_{p,v}$	kJ kg^{-1} K^{-1}	molar specific heat of species *i* at constant volume
$c_{p,m}$	kJ kg^{-1} K^{-1}	molar specific heat of species *i* at constant volume
d	m	depth of head fire
d_{ig}	m	depth of ignition fire-line
HRR	W	total heat release rate
Δh_{pyr}	kJ kg^{-1}	heat of pyrolysis of the vegetative fuel
h_s	m	height of solid fuel
Δh_c	kJ kg^{-1}	mass-based heat of combustion
$\Delta \bar{h}_c$	kJ mol^{-1}	molar-based heat of combustion
I	kW m^{-1}	fireline intensity
I_R	kW m^{-2}	reaction intensity
L_{ig}	m	length of ignition line
M	–	fuel moisture content as fraction of oven-dried fuel mass (expressed as a percentage)
m''_s	kg m^{-2}	mass loading of dry vegetative fuel
$m''_{s,m}$	kg m^{-2}	mass loading of moisture in vegetative fuel
$\dot{m}''_s$	kg m^{-2} s^{-1}	mass loss rate
$\dot{m}''_{s,m}$	kg m^{-2} s^{-1}	mass loss rate of moisture
$\dot{m}''_{s,pyr}$	kg m^{-2} s^{-1}	mass flux of fuel gas due to pyrolysis of vegetative solid fuel
N_L	–	number of layers in model of vegetation
R_o	m s^{-1}	experimentally observed head fire spread rate
R_s	m s^{-1}	empirically derived potential quasi-steady head fire spread rate
$\dot{q}''_c$	kW m^{-2}	convective flux
$\dot{q}''_{sr}$	kW m^{-2}	net radiative flux
T	°C	temperature (*a* ambient, *g* gas phase, *s* solid)
t	s	time
$\boldsymbol{u}$	m s^{-1}	velocity vector
w_s	kg m^{-2}	vegetative fuel loading
$U(z)$	m s^{-1}	dependence of the ambient wind with height
U_2	m s^{-1}	wind speed in direction of spread at 2 m above ground
$U_{2,i}$	m s^{-1}	initial wind speed in direction of spread at 2 m above ground
x, y	m	position vector
Δx, Δy, Δz	m	length of computational cell in x, y, z directions
W	m	width of head fire
w_s	kg m^{-2}	vegetative fuel loading
z	m	height above ground
β_s	–	
σ_s	m^{-1}	surface-to-volume ratio of fuel elements
ρ_s	kg m^{-3}	fuel particle density
ρ_{sb}	kg m^{-3}	bulk density of solid fuel
τ	s	residence time
χ_{char}	–	fraction of virgin solid fuel converted to char
χ_r	–	fraction of local chemical heat release radiated to surroundings
χ_s	–	fraction of consumed fuel mass converted to soot